The role of kinetochore dynein in checkpoint silencing is restricted to disassembly of the corona

Amy H. Ide, Keith F. DeLuca, O'Neil Wiggan, Steven M. Markus*, and Jennifer G. DeLuca* Department of Biochemistry and Molecular Biology, Colorado State University, Fort Collins, Colorado 80523

ABSTRACT During mitosis, kinetochore–microtubule attachments are monitored by a molecular surveillance system known as the spindle assembly checkpoint. The prevailing model posits that dynein evicts checkpoint proteins (e.g., Mad1, Mad2) from stably attached kinetochores by transporting them away from kinetochores, thus contributing to checkpoint silencing. However, the mechanism by which dynein performs this function, and its precise role in checkpoint silencing remain unresolved. Here, we find that dynein's role in checkpoint silencing is restricted to evicting checkpoint effectors from the fibrous corona, and not the outer kinetochore. Dynein evicts these molecules from the corona in a manner that does not require stable, end-on microtubule attachments. Thus, by disassembling the corona through indiscriminate microtubule encounters, dynein primes the checkpoint signaling apparatus so it can respond to stable end-on microtubule attachments and permit cells to progress through mitosis. Accordingly, we find that dynein function in checkpoint silencing becomes largely dispensable in cells in which checkpoint effectors are excluded from the corona.

Monitoring Editor Kerry Bloom University of North Carolina at Chapel Hill

Received: Apr 17, 2023 Accepted: Apr 20, 2023

INTRODUCTION

A critical aspect of mitotic cell division is the accurate and reliable segregation of genetic material. This requires that each of the two sister kinetochores on a mitotic chromosome generate stable attachments to microtubule plus ends emanating from opposite spindle poles before anaphase onset. To ensure this occurs with a high degree of fidelity, cells have evolved a surveillance mechanism referred to as the spindle assembly checkpoint (SAC; London and Biggins, 2014b; Gorbsky, 2015; Lischetti and Nilsson, 2015; Sacristan

This article was published online ahead of print in MBoC in Press (http://www.molbiolcell.org/cgi/doi/10.1091/mbc.E23-04-0130) on April 26, 2023.

Author contributions: J.G.D. and S.M.M. designed the study and wrote the manuscript. A.H.I. performed and analyzed all of the assays and generated most of the figures. K.F.D. provided technical support. O.W. and A.H.I. generated the CRISPR/Cas9 DHC-GFP cell line. All authors participated in revising and editing the figures and manuscript.

*Address correspondence to: Steven M. Markus (steven.markus@colostate.edu); Jennifer G. DeLuca (jennifer.deluca@colostate.edu).

Abbreviations used: APC/C, anaphase promoting complex/cyclosome; DHC, dynein heavy chain; DIC, differential interference microscopy; IF, immunofluorescence; KMN, KNL1-Mis12-NDC80 complex; MCC, mitotic checkpoint complex; Nz, nocodazole; RZZ, Rod-Zwilch-ZW10 complex; SAC, spindle assembly checkpoint; SD, standard deviation.

© 2023 Ide et al. This article is distributed by The American Society for Cell Biology under license from the author(s). Two months after publication it is available to the public under an Attribution–Noncommercial-Share Alike 4.0 International Creative Commons License (http://creativecommons.org/licenses/by-nc-sa/4.0). "ASCB®," "The American Society for Cell Biology®," and "Molecular Biology of the Cell®" are registered trademarks of The American Society for Cell Biology.

and Kops, 2015; Pesenti et al., 2016; Musacchio and Desai, 2017; Kops et al., 2020; Lara-Gonzalez et al., 2021). Kinetochores lacking stable microtubule attachments recruit a suite of SAC proteins that catalyze the formation of a diffusible "wait anaphase" complex that prevents mitotic progression by inhibiting the anaphase promoting complex/cyclosome (APC/C), an E3 ubiquitin ligase whose action is required for progression into anaphase (Chang et al., 2015; Gorbsky, 2015; Lischetti and Nilsson, 2015; Sacristan and Kops, 2015; Pesenti et al., 2016; Alfieri et al., 2017; Heasley et al., 2017; Musacchio and Desai, 2017; Kops et al., 2020; Lara-Gonzalez et al., 2021). These inhibitory mitotic checkpoint complexes, or MCCs, are comprised of the kinetochore-associated proteins Mad2, BubR1, and Bub3, as well as Cdc20, the mitotic cofactor/activator of the APC/C (Sudakin et al., 2001; Herzog et al., 2009; Chao et al., 2012; Alfieri et al., 2016; Di Fiore et al., 2016). Upon establishment of proper attachment to spindle microtubules, SAC proteins are evicted from kinetochores, which results in cessation of MCC assembly, loss of the "wait anaphase" signal, and consequent progression into anaphase (Wang et al., 2014; Agarwal and Varma, 2015; Etemad and Kops, 2016; Lara-Gonzalez et al., 2021).

Silencing of this checkpoint, which is required for anaphase onset and mitotic exit, is thought to be initiated by the eviction of Mad1, a key checkpoint effector that recruits the MCC protein Mad2 to unattached kinetochores (Chen et al., 1998; Hoffman et al., 2001; Luo et al., 2002; Sironi et al., 2002; De Antoni et al., 2005;

Firestone et al., 2012; Ballister et al., 2014). Although it is known that stable, end-on kinetochore-microtubule attachments result in removal of Mad1 and Mad2, the precise molecular events that trigger their eviction remain unclear. Checkpoint proteins are recruited to kinetochores by several distinct pathways (Silio et al., 2015), and accordingly, multiple mechanisms are thought to result in their removal. For example, Mad1 and Mad2 are recruited to the outer kinetochore by the kinetochore-associated proteins KNL1 and Bub1, and also by the Rod/Zwilch/ZW10 (RZZ) complex (Brady and Hardwick 2000; Buffin et al., 2005; Kops et al., 2005; London and Biggins, 2014a; Ji et al., 2017; Zhang et al., 2017; Fischer et al., 2021; Lara-Gonzalez et al., 2021). Mad1 and Mad2 are additionally recruited by cyclin B1 to a region of the kinetochore known as the fibrous corona (Allan et al., 2020). In light of these distinct recruitment pathways, it is unsurprising that at least two mechanisms are thought to mediate removal of Mad1 and Mad2 from kinetochores: 1) loss of kinetochore binding sites through phosphatase activity (hereafter referred to as the phosphatase pathway) and 2) transport along microtubules by the minus end-directed microtubule motor cytoplasmic dynein-1 (hereafter referred to as the dynein pathway). The former occurs in response to changes in the phosphorylation status of key kinetochore proteins, such as the MELT motifs on the kinetochore scaffold protein KNL1. It is well established that phosphorylation of these motifs by the Mps1 kinase is required for the recruitment of the checkpoint proteins Bub3, BubR1, and Bub1 (Larsen et al., 2007; London et al., 2012; Shepperd et al., 2012; Yamagishi et al., 2012; Primorac et al., 2013; Ji et al., 2017). Mps1 has also been shown to phosphorylate Bub1, which directly recruits a population of Mad1 to kinetochores (London and Biggins, 2014a; Ji et al., 2017; Zhang et al., 2017; Fischer et al., 2021). Upon microtubule attachment, Mps1 is evicted from kinetochores (Hiruma et al., 2015; Ji et al., 2015) and kinetochore phosphatases reverse Mps1mediated phosphorylation events, leading to loss of kinetochore binding sites for Bub1 and Mad1 (Nijenhuis et al., 2014; Saurin, 2018; Moura and Conde, 2019; Garvanska and Nilsson, 2020).

Although how the dynein pathway precisely contributes to checkpoint silencing is poorly understood, dynein itself localizes prominently to unattached kinetochores, and delocalizes as kinetochores encounter microtubules (Pfarr et al., 1990; Steuer et al., 1990; King et al., 2000; Howell et al., 2001). Given the minus enddirected motility of this motor protein, the prevailing model posits that dynein actively evicts Mad1, Mad2, and other proteins from properly attached kinetochores by transporting them as cargoes toward the spindle poles (Pfarr et al., 1990; Steuer et al., 1990; King et al., 2000; Hoffman et al., 2001; Howell et al., 2001; Bader and Vaughan, 2010; Wang et al., 2014; Agarwal and Varma, 2015; Lara-Gonzalez et al., 2021). Processive dynein motility requires its activating complex dynactin (for dynein activator) and a cargo adaptor molecule (e.g., Hook3, BicD2) that links dynein and dynactin to each other and to their cargo (McKenney et al., 2014; Schlager et al., 2014). The kinetochore-localized adaptor protein Spindly (McKenney et al., 2014; d'Amico et al., 2022), which localizes to kinetochores via the RZZ complex (Gassmann et al., 2008, 2010; Barisic et al., 2010; Gama et al., 2017; Mosalaganti et al., 2017; Sacristan et al., 2018), has been implicated in providing this function, as mutations that disrupt its interaction with dynein and dynactin strongly reduce their kinetochore association (Gassmann et al., 2010; Sacristan et al., 2018). Consistent with a role for dynein in checkpoint silencing, cells expressing such Spindly mutants exhibit increased kinetochore association of Mad1 and Mad2 at metaphase, and a prolonged mitotic arrest (Barisic et al., 2010; Gassmann et al., 2010). Complicating our understanding of dynein and Spindly in checkpoint silencing, however, is the fact that Mad2 delocalizes from aligned kinetochores in cells in which Spindly is depleted (Chan et al., 2009; Gassmann et al., 2010). Moreover, these cells only exhibit a modest checkpoint delay. Thus, kinetochore dynein becomes dispensable for checkpoint silencing in cells without Spindly. Reconciling these seemingly contradictory findings is important to understand the roles of dynein and Spindly in the establishment and silencing of the spindle assembly checkpoint.

It is important to note that a number of SAC effectors, including Mad1, Mad2, Spindly, RZZ, and dynein-dynactin, are localized to a proteinaceous outer region of the kinetochore that is unique to those that are unattached: the fibrous corona (Kops and Gassmann, 2020). In conditions whereby kinetochores are experimentally prevented from attaching to microtubules (e.g., in the presence of the microtubule depolymerizing agent nocodazole), the corona significantly expands into large crescent-shaped structures, and in some cases nearly full rings that circumscribe the sister kinetochores (Ris and Witt, 1981; Rieder, 1982; Thrower et al., 1996; Hoffman et al., 2001; Wynne and Funabiki, 2015). The prevailing model for corona function is that it promotes kinetochore-microtubule attachments by enabling lateral encounters between corona-localized microtubule-binding proteins (e.g., dynein, CENP-F, and CENP-E) and microtubules (Magidson et al., 2011; Sacristan et al., 2018; Kops and Gassmann, 2020). Such encounters, which are ultimately converted to mature end-on attachments, accelerate spindle assembly by several minutes (Magidson et al., 2011). In spite of the presence of Mad1 and Mad2 within the meshwork of the corona, it is currently unclear whether these corona-localized SAC effectors are capable of signaling a mitotic arrest. Although it has been postulated that the corona functions in checkpoint signaling (Allan et al., 2020; Kops and Gassmann, 2020), some evidence suggests otherwise (Rodriguez-Rodriguez et al., 2018). Finally, recent studies have found that the RZZ complex and the dynein adaptor Spindly are all required for expansion of the corona, while dynein, which is recruited by Spindly, is required for disassembly of this structure (Sacristan et al., 2018).

Central among the unanswered questions regarding kinetochore dynein function are the following: 1) What is dynein's precise role in checkpoint silencing? 2) Given the localization of SAC proteins to both the fibrous corona and the outer kinetochore, is dynein activity restricted to removing only a certain population? 3) How are these motors activated to evict SAC effectors (i.e., does dynein sense and respond to kinetochore-microtubule attachment status)? With respect to this latter question, early experiments suggested that "mature," end-on microtubule attachments were not in fact required to initiate this process, but that lateral or transient kinetochore-microtubule attachments were sufficient. For example, observations of the rapid reduction in kinetochore dynein levels shortly after nuclear envelope breakdown—well before stable attachments are established—supported this idea (King et al., 2000; Howell et al., 2001). In addition, it has been shown that Mad2 eviction from kinetochores occurs in cells lacking NDC80 complex components and thus lacking stable kinetochore-microtubule attachments (DeLuca et al., 2003). Such observations suggested that dynein need not be activated, per se, but that it simply requires a microtubule on which to walk. However, more recent studies have refuted this idea, and suggested that stable, end-on attachments are indeed required for dynein to remove SAC protein cargo, and that lateral attachments are not sufficient (Magidson et al., 2015; Kuhn and Dumont, 2017). Determining the means by which dynein is activated to evict SAC effectors, and which population(s) it evicts, will yield important insight into the mechanism by which this motor

senses and/or responds to chromosome alignment status and mitotic progression.

In this study, we set out to determine the role of the dynein pathway in eviction of SAC effectors from kinetochores. We find that dynein's role is restricted to removing proteins from the fibrous corona, and not the outer kinetochore. We also find that SAC effectors within the corona are capable of signaling a checkpoint arrest from a small number of unaligned chromosomes, and thus prevent chromosome segregation errors in such situations. Finally, our results indicate that dynein function in the eviction of SAC proteins and in checkpoint silencing becomes largely dispensable in cells in which SAC effectors can no longer accumulate at the corona. Based on our data, we posit that the phosphatase pathway triggers SAC protein removal only in response to kinetochore-microtubule attachment status, whereas dynein functions to prime kinetochores for checkpoint silencing by specifically removing corona-localized SAC effectors through indiscriminate encounters with microtubules.

RESULTS

The majority of kinetochore Mad2 is evicted by the phosphatase pathway

The SAC protein Mad2 is thought to be evicted from kinetochores by at least two mechanisms: 1) loss of its kinetochore recruitment factor, Mad1, in response to dephosphorylation events including those on Bub1 and KNL1 (hereafter referred to as the phosphatase pathway), and 2) transport away from kinetochores by the minus end-directed microtubule motor dynein. Although initiation of both of these pathways requires the presence of spindle microtubules during an unperturbed mitosis, the precise role for microtubules in these pathways, and the extent to which each pathway contributes to Mad2 eviction are unknown. To begin to determine the contribution of each of these two mechanisms to the eviction of Mad2 from kinetochores, we devised the following experimental scheme (Figure 1A). Untransfected cells, or those expressing Mad2-GFP were arrested in prometaphase by treatment with 5 μM nocodazole for 16 h, which depolymerizes all spindle microtubules (see Figure 3A), and results in maximal Mad2 levels at kinetochores (see Figure 1, E and F; t = -2.5 min). Checkpoint silencing was then initiated by treatment with reversine, an inhibitor of the checkpoint kinase Mps1, which prevents phosphorylation of its multiple kinetochore targets, including the KNL1 MELT repeats and Bub1 (Santaguida et al., 2010; London et al., 2012; Shepperd et al., 2012; Yamagishi et al., 2012; Ji et al., 2017; Fischer et al., 2021; Lara-Gonzalez et al., 2021). This treatment mimics the loss of Mps1 from kinetochores which, in unperturbed cells occurs in response to the establishment of stable, end-on microtubule attachments (Hiruma et al., 2015; Ji et al., 2015). Reversine addition is sufficient to silence the SAC and promote mitotic exit, even in situations in which there is a complete absence of microtubules (Santaguida et al., 2010). For most experiments, cells were also treated with the proteasome inhibitor MG132, which precludes anaphase onset by preventing APC/C-dependent degradation of cyclin B1 and securin. Cells were then either imaged over time using fluorescence microscopy to monitor Mad2-GFP levels at kinetochores, or were fixed 2 h after reversine treatment, and processed for immunofluorescence.

To establish the appropriate conditions for this assay, we treated cells with either low (500 nM) or high (10 µM) concentrations of reversine, and immunostained cells using antibodies against phosphorylated MELT domains in KNL1 (pMELT), which are direct targets of Mps1 (London et al., 2012; Shepperd et al., 2012; Yamagishi et al., 2012; Vleugel et al., 2013). Whereas treatment with 500 nM reversine reduced pMELT levels by 48.5%, 10 µM led to a 72.4% reduction

(Figure 1B). Because of the more pronounced reduction in pMELT by 10 µM reversine, we chose to use this concentration for subsequent assays. Consistent with previous studies, in the absence of MG132 and in the presence of 5 μM nocodazole, treatment with this high concentration of reversine led to loss of cyclin B1 (Figure 1C), and mitotic exit approximately 63 min after addition of the drug (Figure 1D), indicating the time required by the phosphatase pathway to promote mitotic progression under these conditions.

Fluorescence intensity measurements from time-lapse movies revealed that treatment with 10 µM reversine results in approximately 74% of kinetochore-associated Mad2 being evicted within 2 h, with the majority being removed within the first few minutes (Figure 1, E and F). Nearly identical results were obtained from our fixed-cell experiments, in which cells were treated with 5 µM nocodazole for 16 h, followed by the addition of reversine and MG132 for 2 h, and then processed for immunofluorescence (Figure 1A, bottom, and 1G). Consistent with our pMELT staining, we noted a greater reduction in Mad2 levels with high reversine treatment. Given the complete lack of microtubules in these cells, these data suggest that the eviction of this majority population of Mad2 is due to activation of the phosphatase pathway, which eliminates binding sites for Bub3/Bub1 on KNL1 (Saurin, 2018).

In contrast to Mad1 and Mad2, the SAC effector BubR1 has not been implicated as a dynein cargo (Howell et al., 2004; Famulski et al., 2011), and thus is presumably evicted entirely via the phosphatase pathway. Much like Mad1/Mad2, however, BubR1 is recruited to kinetochores in a manner that requires phosphorylation of the KNL1 MELT motifs. Intensity measurements of nocodazole and reversine-treated BubR1-GFP-expressing cells revealed that BubR1 was reduced to almost undetectable levels within 10 min of reversine addition (Figure 1, H and I). These results are consistent with the notion that BubR1 is not a cargo of kinetochore dynein, and its eviction from kinetochores likely occurs exclusively via dephosphorylation of kinetochore substrates of Mps1. Taken together, our data suggest that the majority of Mad2 is evicted from kinetochores as a consequence of dephosphorylation of kinetochore substrates, while a minority relies on other means.

Dynein is required for the eviction of a minority population of kinetochore Mad2

We hypothesized that the population of kinetochore Mad2 remaining after reversine treatment is a consequence of dynein having no microtubules on which to walk. To test this idea, we employed a Spindly mutant that is unable to recruit dynein to kinetochores (Gassmann et al., 2010). A previous study showed that Mad1 and Mad2 are retained at aligned kinetochores in cells expressing Spindly^{F258A}, which perturbs one of three dynein-dynactin-binding domains in Spindly (Gassmann et al., 2010; Sacristan et al., 2018). Here, we employed a Spindly mutant in which all three dynein-dynactin-binding domains are perturbed (Spindly^{ACCS}) (Sacristan et al., 2018). The levels of Mad2 at kinetochores in early prometaphase and metaphase cells expressing either wild-type Spindly or Spindly $^{\Delta CCS}$ were measured. Consistent with a role for Spindly in recruiting dynein-dynactin to kinetochores, cells expressing Spindly^{ACCS} exhibited significantly reduced levels of the dynactin component p150Glued at early prometaphase kinetochores (Figure 2, A-C). Whereas cells expressing wild-type Spindly exhibited a 94% reduction in kinetochore Mad2 levels from early prometaphase to metaphase, those expressing Spindly $^{\Delta CCS}$ only exhibited a 78% reduction, suggesting that dynein is required for eviction of only 16% of Mad2 (Figure 2, D and E). In contrast to Mad2, we found that Mps1 is not evicted as a consequence of dynein activity by comparing the relative extent of phosphorylated KNL1 MELT

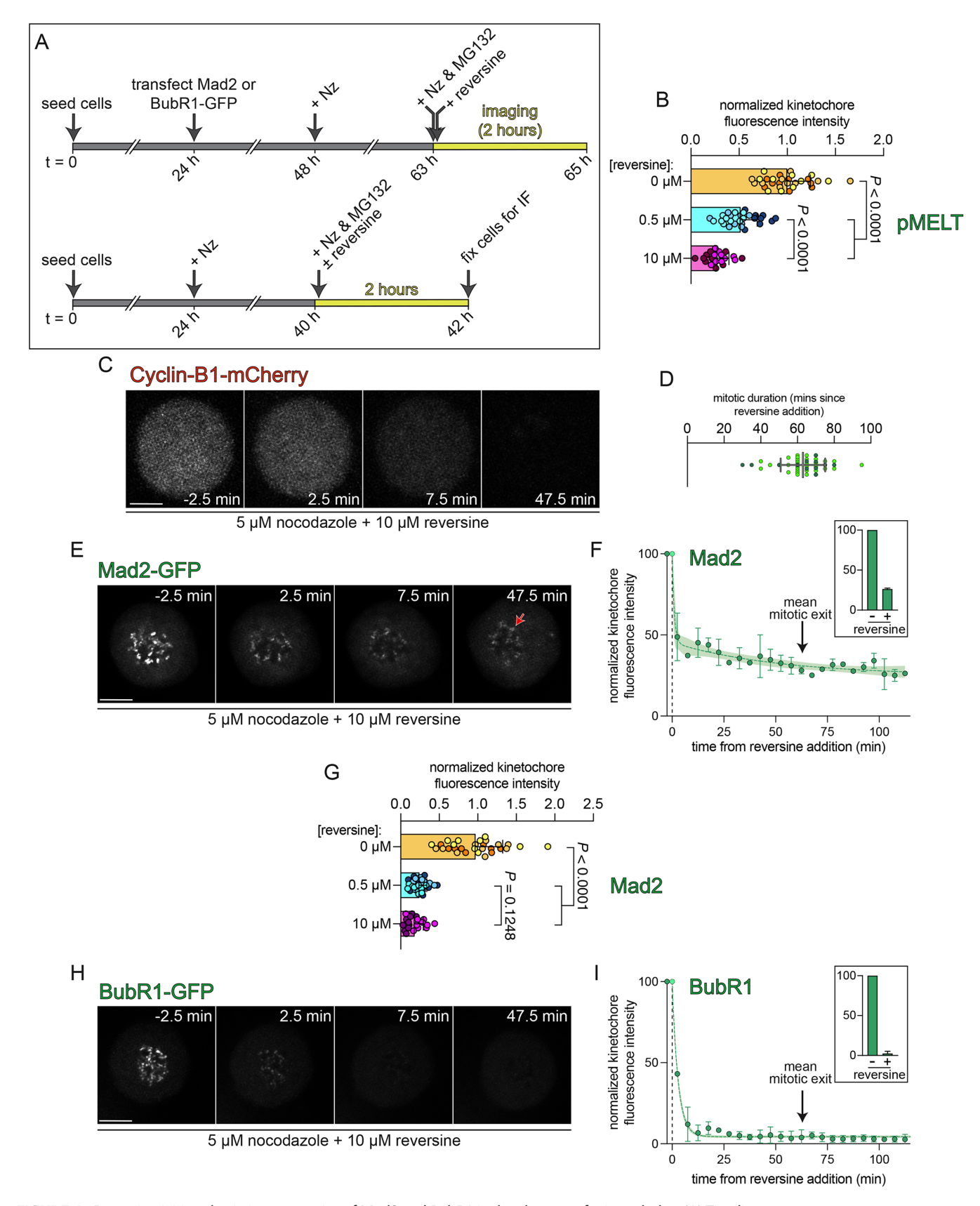


FIGURE 1: Reversine-initiated eviction properties of Mad2 and BubR1 in the absence of microtubules. (A) Timeline of workflow for live-cell (top) and fixed-cell (bottom) experiments (Nz, nocodazole; IF, immunofluorescence). (B) Normalized fluorescence intensity levels of kinetochore-associated phospho-MELT (pMELT) staining in fixed cells treated with indicated concentration of reversine (n = 58 cells from 3 replicates for 0 and 0.5 μ M reversine conditions, 20 cells from 2 replicates for 10 μ M reversine condition). (C) Representative time-lapse images of live cyclin-B1-mCherry-expressing HeLa cells

motifs (i.e., pMELT) at early prometaphase and metaphase kinetochores in cells expressing either wild-type Spindly or Spindly^{△CCS} (Figure 2F). Taken together with our findings described above, these results suggest that a majority of Mad2 (~74-84%) is evicted from kinetochores by the phosphatase pathway (which is triggered by stable kinetochore-microtubule attachments during an unperturbed mitosis), while only a small population requires dynein.

To further investigate the eviction requirements of this dyneindependent population, we sought to determine the extent to which kinetochore Mad2 is reduced in cells in which the dynein pathway is active, but the phosphatase pathway is inhibited. To this end, we measured the extent of Mad2 reduction in cells containing short microtubule "tufts" in the vicinity of kinetochores and chromosomes. We reasoned that such microtubules, generated with lower (0.5 μ M) concentrations of nocodazole (Figure 3A), would provide dynein with tracks on which it could transport Mad2 away from kinetochores. However, these tufts are likely insufficient to establish the stable attachments to kinetochores that are required to robustly trigger the phosphatase pathway, and thus silence the SAC (Etemad et al., 2015; Hiruma et al., 2015; Ji et al., 2015; Tauchman et al., 2015). As shown in Figure 3B, a 16 h incubation in 0.5 μM nocodazole results in a significant reduction in kinetochore-associated Mad2 (relative to 5 µM nocodazole-treated cells), suggesting that the presence of these microtubule tufts is sufficient to initiate eviction of Mad2, likely as a consequence of dynein motility. Subsequent treatment of these cells with reversine reduced Mad2 to undetectable levels, indicating that the remaining kinetochore-associated Mad2 molecules require the phosphatase pathway for removal (compared with an ~70% reduction of Mad2 after reversine addition to cells treated with 5 μ M nocodazole; Figure 3B).

Notably, the extent of the tuft-initiated Mad2 eviction was greater than expected based on our data with Spindly^{ACCS} (Figure 2E). One possibility to account for this greater than expected reduction in Mad2 is that the tufts are capable of establishing weak and/ or transient end-on attachments that are sufficient to evict a fraction of Mps1 by inducing architectural changes within the kinetochore (Etemad et al., 2015; Tauchman et al., 2015), thus partially activating

the phosphatase pathway. To determine whether this was the case, we assessed the extent of Mps1 phosphorylation of the KNL1 MELT motifs (pMELT)—a readout for the phosphatase pathway—after treating cells with either 5 or 0.5 μM nocodazole for 16 h (London et al., 2012; Shepperd et al., 2012; Zhang et al., 2017). This revealed that the levels of Mps1 phosphorylation of KNL1 are 43.2% lower after incubating cells in 0.5 µM nocodazole compared with 5 µM nocodazole-treated cells (Figure 3C), indicating that kinetochore Mps1 levels are reduced by the presence of microtubule tufts. Thus, some of the Mad2 eviction noted in Figure 3B (~43%) can indeed be accounted for by the activation of the phosphatase pathway by microtubule tufts, whereas the remaining ~24% is likely due to dynein indiscriminately evicting Mad2 as a consequence of kinetochores encountering a microtubule track.

Taken together, these results demonstrate that the checkpoint effector Mad2 is evicted from kinetochores by at least two mechanisms: 1) one that results from loss of sustained Mps1 activity and subsequent kinetochore substrate dephosphorylation (the phosphatase pathway), and 2) one that relies on dynein-mediated transport activity along kinetochore-associated microtubules. Further, they suggest that indiscriminate microtubule encounters with kinetochores (e.g., nonstable attachments) are sufficient to evict some fraction of SAC effectors from kinetochores.

Dynein specifically evicts corona-associated Mad2 from kinetochores

Mad2 has been mapped to at least two distinct locations within the kinetochore: 1) the outer kinetochore, which contains the "KMN" (KNL1/Mis12 complex/Ndc80 complex) network that is responsible for the force-transducing microtubule-binding activity at kinetochores, and 2) the fibrous corona, which is an expandable meshwork of proteins assembled on the outer kinetochore (Kops and Gassmann, 2020). In light of the contribution of both the phosphatase and dynein pathways to Mad2 eviction, we wondered whether dynein specifically removes one of these populations of Mad2, while the phosphatase pathway removes the other. To test this idea, we assessed the role of the dynein pathway in Mad2 eviction in cells

treated with 5 μ M nocodazole for 16 h, and then treated with 10 μ M reversine (at time = 0 min) during imaging. (D) Mitotic duration (for experiment shown in panel C) as determined from the reduction in cyclin-B1-mCherry fluorescence levels to undetectable levels (n=47 cells from 2 independent replicates, which are indicated by different shades of green). Mean \pm SD is shown. (E, F) Representative images and quantitation of live Mad2-GFP-expressing HeLa cells imaged before and after the addition of 10 µM reversine (added at time = 0). Red arrow indicates residual Mad2 signal remaining at kinetochores 47.5 min after reversine addition. Normalized and photobleaching-corrected fluorescence intensity levels of Mad2-GFP are plotted (n = 23 cells from 2 replicates). Black arrow indicates the average mitotic duration following reversine treatment, as shown in panel D. The data were fit (green dashed line; overlaid with 95% confidence interval indicated with shaded green) to a two-phase exponential decay with $t_{1/2}^1 = 34.0$ min, and $t_{1/2}^2 = 1.3$ min ($R^2 = 0.96$). (G) Normalized fluorescence intensity levels of kinetochore-associated endogenous Mad2 (via immunostaining) in cells treated with indicated concentration of reversine (n = 59 cells from 3 replicates for 0 and 0.5 μ M reversine conditions, 20 cells from 2 replicates for 10 µM reversine condition). (H, I) Representative images and quantitation of BubR1-GFPexpressing HeLa cells imaged before and after the addition of 10 µM reversine (added at time = 0). Note the lack of fluorescence signal remaining at kinetochores within 7.5 min of reversine addition. Normalized and photobleachingcorrected fluorescence intensity levels of BubR1-GFP are plotted (n = 17 cells from two replicates). Black arrow indicates the average mitotic duration following reversine treatment, as shown in panel D. The data were fit (green dashed line; overlaid with 95% confidence interval indicated with shaded green) to a one-phase exponential decay with $t_{1/2} = 2.0$ min $(R^2 = 0.99)$. To account for the time lag between acquiring the prereversine image and the first postreversine image (~2.5 min), we assumed the intensity values for the 0 time point for Mad2- and BubR1-GFP were equal to that of the prereversine addition time point (dashed light-green circle). Insets for both F and I indicate mean normalized intensity of Mad2- and BubR1-GFP at the beginning (t = -2.5 min) and end (t = 117.5 min) of the imaging period. For panels B and E-I, 10 µM MG132 was included to prevent mitotic exit. All scale bars = 10 µm. Statistical significance was determined by comparing means using Brown-Forsythe and Welch one-way ANOVA tests.

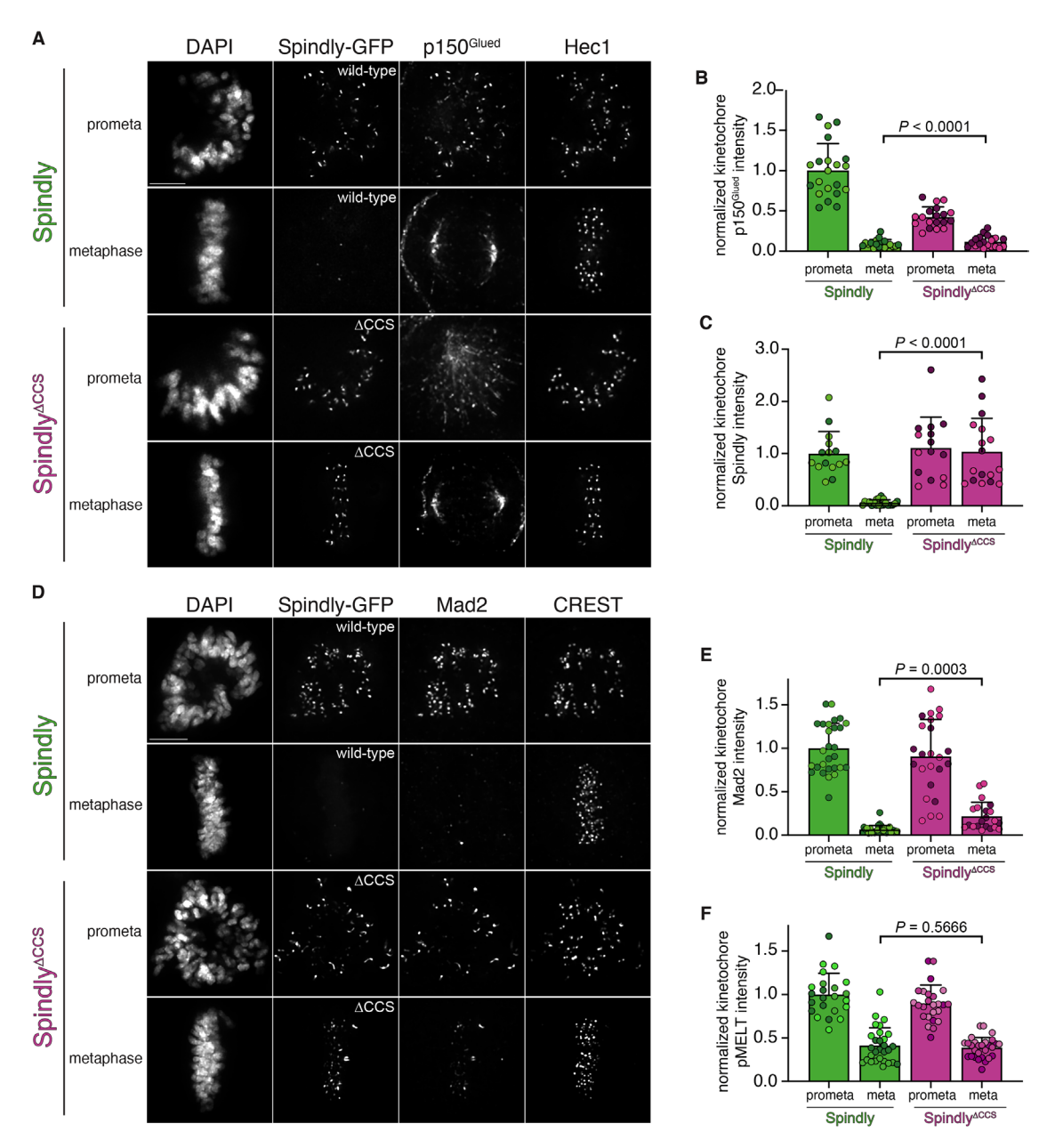


FIGURE 2: Dynein is required for the eviction of a minority population of Mad2 from kinetochores. (A) Representative immunofluorescence images depicting relative Spindly and p150^{Glued} levels in either early prometaphase ("prometa") or metaphase cells (identified from an asynchronous population) depleted for Spindly and expressing either wild-type or mutant Spindly, as depicted. (B, C) Plots depicting normalized kinetochore p150^{Glued} or Spindly intensity levels in cells shown in panel A (n = 1560 kinetochores from 78 cells from 2 replicates for p150; 1340 kinetochores from 67 cells from 2 replicates for Spindly). (D) Representative immunofluorescence images depicting relative Spindly and Mad2 levels in either early prometaphase or metaphase cells (identified from an asynchronous population) expressing either wild-type or mutant Spindly. (E) Plot depicting normalized kinetochore Mad2 intensity levels in cells shown in panel D (n = 2020 kinetochores from 101 cells, from 2 replicates). (F) Plots depicting normalized kinetochore pMELT (antibody directed at phosphorylated KNL1) intensity levels for early prometaphase or metaphase cells expressing either wild-type or mutant Spindly, as depicted (n = 2100 kinetochores from 105 cells from 3 replicates). All scale bars = 5 µm. Statistical significance was determined by comparing means using a Student's t test with Welch's correction.

that are compromised for assembly of the fibrous corona. We reasoned that if dynein's role is to evict only the corona population, then eliminating the corona would obviate the need for dynein-mediated removal of kinetochore Mad2 along microtubules. To this end, we depleted cells of Spindly, which leads to significantly reduced coronas even in the presence of 5 μ M nocodazole (Figure 4, A and B; Sacristan et al., 2018). In the control experiment, the addi-

tion of reversine to nocodazole-treated cells reduced Mad2 to 30.2%. However, the addition of reversine to nocodazole-treated cells depleted for Spindly reduced Mad2 to undetectable levels (Figure 4, C and D). This total loss of Mad2 from kinetochores by reversine in spite of the complete absence of microtubules supports the notion that the corona population of Mad2 is the only population removed by the dynein pathway.

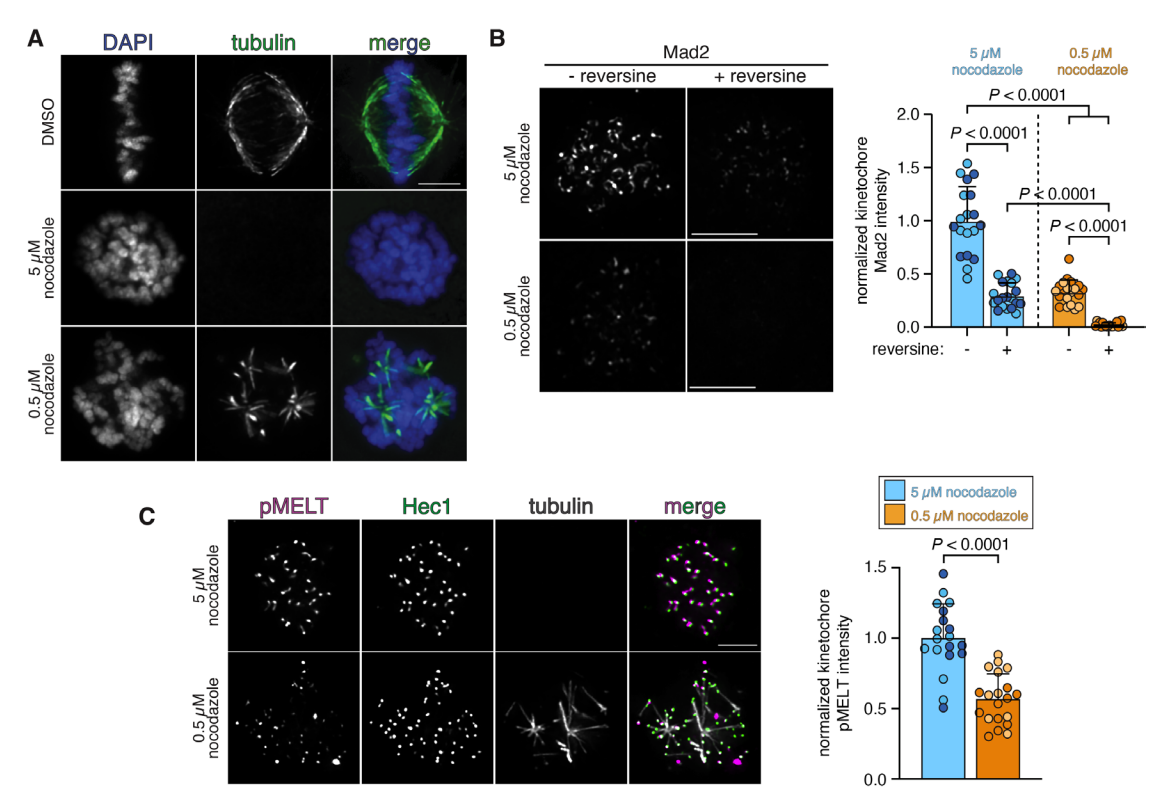


FIGURE 3: Microtubule tufts are sufficient to evict a subpopulation of Mad2 from kinetochores. (A) Representative immunofluorescence images depicting the degree of microtubule depolymerization by 5.0 and 0.5 µM nocodazole. Cells were incubated overnight in the indicated concentration of nocodazole, and then processed for immunofluorescence. Note the presence of microtubule "tufts" after incubation in 0.5 µM nocodazole, but a complete lack of microtubules after incubation in 5.0 µM nocodazole. (B) Representative images and quantitation of cells treated overnight with the indicated concentration of nocodazole, and then either processed for immunofluorescence, or treated for an additional 2 h with 10 μ M reversine (plus MG132) and then processed for immunofluorescence. Plot (means \pm SD) indicates relative kinetochore Mad2 levels in cells treated as indicated (n = 1580 kinetochores from 79 cells, 2 replicates; different shades of blue and orange indicate different replicates). (C) Representative images of cells treated overnight with the indicated concentration of nocodazole, and then processed for immunofluorescence to determine extent of KNL1 MELT phosphorylation. Plot (means \pm SD) indicates relative kinetochore pMELT levels in cells treated as indicated (n = 380kinetochores from 19 cells). All scale bars = 5 µm. Statistical significance was determined by comparing means using Brown-Forsythe and Welch one-way ANOVA tests (B) or by comparing means using a Student's t test with Welch's correction (C).

To confirm the above findings, and to use an experimental approach that does not impact the recruitment of dynein to kinetochores (as Spindly depletion does; Gassmann et al., 2010), we used a CRISPR/Cas9-generated Mad1 knockout cell line expressing either transgenic wild-type Mad1 or a mutant version of Mad1, Mad1^{3EK}. This mutant is compromised in its ability to bind coronalocalized cyclin B1, but localizes normally to the outer kinetochore (Allan et al., 2020). We treated these cells with either 5 µM nocodazole and MG132, or 5 µM nocodazole plus 10 µM reversine and MG132. As expected, Mad2 failed to localize to the corona in the Mad1 3EK -expressing cells after treatment with 5 μM nocodazole and MG132, and instead was observed as paired dots, indicative of localization only to the outer kinetochore (Figure 4E; see insets). Whereas treating wild-type cells with reversine reduced kinetochore Mad2 levels to 39%, the same treatment of Mad1^{3EK}-expressing cells reduced Mad2 at the kinetochore to almost undetectable levels (Figure 4, E and F). These results, which are consistent with our Spindly depletion data, support the idea that the population of Mad2 that relies on the dynein pathway for eviction specifically resides at the corona and not the outer kinetochore.

If the dynein pathway is solely responsible for evicting the corona-localized population of SAC effectors from kinetochores, this would suggest that the phosphatase pathway plays little to no role in eviction of checkpoint proteins from the corona. Thus, dynein and its cargoes at the corona would be predicted to be largely refractory to reversine treatment. To test this idea, we assessed the localization dynamics of kinetochore-associated dynein using a CRISPR/Cas9engineered HeLa cell line in which the dynein heavy chain (DYNC1H1) is endogenously tagged with mClover at its C terminus (hereafter referred to as DHC-mClover). Time-lapse imaging of these cells revealed that they progress through mitosis normally, with an average time from nuclear envelope breakdown to anaphase of 44 \pm 19 min (mean \pm SD; n = 13 cells; see Figure 5A for representative images). Consistent with previous observations, treating DHC-mClover cells with high concentrations of nocodazole leads to the accumulation of dynein at the fibrous corona (Figure 5, B and F). Although the addition of reversine reduced total kinetochore dynein levels in cells without microtubules (due to the presence of 5 µM nocodazole; Figure 5, C and E), the morphological appearance of the coronas remained unchanged (Figure 5B, right panels), suggesting that corona-localized dynein is largely refractory

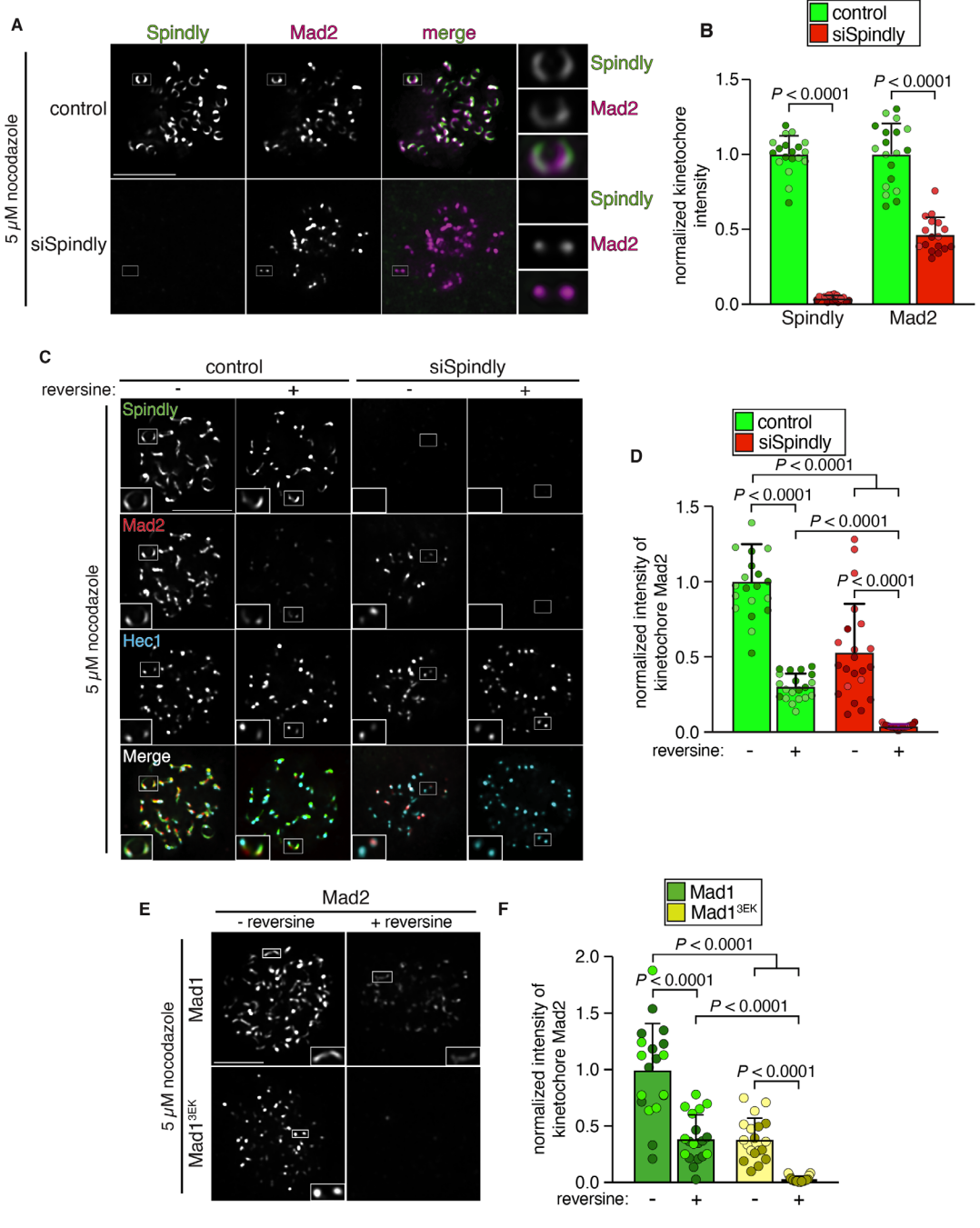


FIGURE 4: The phosphatase pathway is sufficient to evict all kinetochore-associated Mad2 in cells lacking coronas. (A) Representative fluorescence images of Mad2 or Spindly in HeLa cells treated with either control or Spindly siRNA, treated with 5 µM nocodazole for 12 h, and then processed for immunofluorescence. Note the distinct corona morphology in control cells compared with paired dots in the siSpindly treated cells. (B) Plot (means \pm SD) depicting normalized kinetochore levels of Spindly or Mad2 in control or siSpindly treated cells (n ≥ 1440 kinetochores from 72 cells, from 2 replicates; different shades of green and red indicate different replicates). (C, D) Representative fluorescence images and quantitation of Spindly and Mad2 (Hec1 was used as a kinetochore marker) in HeLa cells treated with either control or Spindly siRNA, treated with 5 μ M nocodazole for 12 h, and then either processed for immunofluorescence, or treated with 10 µM reversine (plus MG132) for 2 h before processing. Plot (means ± SD) depicts normalized kinetochore levels of Mad2 in control or siSpindly treated cells ($n \ge 1440$ kinetochores from 72 cells, 2 replicates; different shades of green and red indicate different replicates). (E, F) Representative fluorescence images and quantitation of Mad2 in 5 µM nocodazole-treated cells expressing either wild-type Mad1 or Mad1^{3EK} in cells lacking endogenous Mad1 (see Materials and Methods). Cells were either processed for immunofluorescence after overnight incubation in 5 μ M nocodazole, or treated with 10 μ M reversine (plus MG132) for 2 h before processing. Plot (means \pm SD) depicts normalized kinetochore levels of Mad2 in indicated cells ($n \ge 1600$ kinetochores from 80 cells, 2 replicates; different shades of green and yellow indicate different replicates). Scale bar = 5 µm. Statistical significance was determined by comparing means using a Student's t test with Welch's correction (B), or by comparing means using Brown-Forsythe and Welch one-way ANOVA tests (D and F).

to reversine treatment. Note that we observed similar results with Mad2 and Spindly (see insets for control cells in Figure 4, C and E), and a recent study noted the same for Rod after treatment with the Mps1 inhibitor Cpd-5 (Sacristan et al., 2018). In contrast, overnight incubation of DHC-mClover cells in 0.5 μM nocodazole (to produce microtubule tufts) reduced total kinetochore dynein levels to a greater extent than reversine alone, that was further reduced by the addition of reversine (Figure 5, D and E). Close inspection of the 0.5 μM nocodazole-treated cells revealed that they possessed fewer kinetochores with expanded coronas. Of note, the majority of the corona-free kinetochores were observed in the vicinity of the microtubule tufts, while those with expanded coronas were more likely to be distal from the tufts (Figure 5F, bottom panels). The fact that a population of kinetochores was not in contact with a microtubule tuft—at least at the time of fixation—likely explains the incomplete removal of dynein observed in 0.5 µM nocodazole (Figure 5E). These data indicate that corona-localized dynein, and likely its effectors, are not evicted via the phosphatase pathway, but instead rely on the dynein pathway.

Corona-localized Mad2 contributes to inhibitory "wait anaphase" checkpoint signals

Our results thus far indicate that dynein functions to specifically remove the corona-localized population of Mad2 from kinetochores. In light of previous studies demonstrating a requisite role for dynein in silencing the SAC (Chan et al., 2009; Gassmann et al., 2010), these data suggest that corona-localized Mad2 is capable of generating an inhibitory "wait anaphase" signal. Although recent evidence suggests the corona can indeed signal a checkpoint arrest (Allan et al., 2020), a previous study found that cells deficient in corona expansion (by expressing the mutant Rod^{2A}) exhibit no defects in checkpoint signaling when treated with 660 nM nocodazole (Rodriguez-Rodriguez et al., 2018). Importantly, treatment with this concentration of nocodazole leads to a large number of unattached kinetochores. Therefore, we reasoned that the corona may be dispensable for checkpoint signaling under such conditions, in which the activity of outer kinetochore-localized Mad2 on a large number of unattached kinetochores likely produces a sufficiently strong inhibitory signal to preclude anaphase onset. In contrast, in situations in which the majority of kinetochores are stably attached to microtubules, and only a small number remain unattached, corona-associated Mad2 may become required to generate a sufficiently strong inhibitory signal to arrest anaphase onset. The large number of checkpoint effectors found within a single expanded corona may provide the cell with a sufficiently large number of molecules to generate the inhibitory signal.

To determine whether the corona can indeed generate an inhibitory signal in such situations, we treated cells with a very low dose of nocodazole (25 nM), which causes a small number of misaligned chromosomes per cell (from one to three; Figure 6A, arrows). We used stable cells expressing either wild-type GFP-Rod or GFP-Rod^{2A} (depleted of endogenous Rod) to permit or restrict corona expansion, respectively (Rodriguez-Rodriguez et al., 2018). As a measure of checkpoint function, we assessed mitotic timing in these cells. This revealed that cells expressing wild-type Rod are competent to significantly delay anaphase onset in 25 nM nocodazole; however, cells expressing Rod^{2A} exited mitosis with no checkpoint delay in spite of the presence of unaligned chromosomes (Figure 5, B and C). These results are in contrast to those obtained using cells treated with higher doses of nocodazole (660 nM), in which many kinetochores are unattached, and both wild-type Rod and Rod^{2A}-expressing cells exhibit a robust mitotic arrest (Figure 5B). Of note, consistent with previous studies (Chan et al., 2000; Basto et al., 2004; Famulski et al., 2011), we observed wild-type GFP-Rod clearly accumulating at the spindle poles in wild-type cells. This localization pattern has been attributed to dynein-mediated transport of kinetochore cargoes along microtubules to spindle poles (Figure 6C, top insets; Howell et al., 2001; DeLuca et al., 2003; Chan et al., 2009; Gassmann et al., 2010; Famulski et al., 2011; Silva et al., 2014). This localization pattern was apparent in significantly fewer Rod^{2A}-expressing cells (Figure 6C, bottom insets, and Figure 6D). This lends further support to the notion that dynein's role in checkpoint silencing is restricted to the transport and consequent eviction of coronalocalized effectors, and not those at the outer kinetochore.

To validate the role of the corona in checkpoint silencing, we used the Mad1^{3EK} cells in which Mad1 and Mad2 do not localize to the corona. Consistent with the above results, wild-type Mad1expressing cells exhibited a more robust checkpoint delay in the presence of 25 nM nocodazole than those expressing Mad1^{3EK} (Figure 6E). Much like with the Rod^{2A}-expressing cells, high concentrations of nocodazole were sufficient to induce a robust mitotic delay in Mad13EK-expressing cells, indicating that the checkpoint machinery is largely intact (Figure 6F). Taken together, these findings indicate that the corona is dispensable for SAC signaling in the presence of many unattached kinetochores, but that corona-localized Mad2 becomes essential to initiate a mitotic arrest when there are only a small number of unattached kinetochores.

Dependence on dynein for checkpoint silencing is reduced in the absence of the corona

In light of our findings that the dynein pathway is restricted to evicting checkpoint effectors from the corona, and not the outer kinetochore, we hypothesized that dynein would become dispensable for checkpoint silencing in cells without corona-localized Mad1 and Mad2. To test this idea, we expressed either wild-type Spindly or Spindly^{△CCS} in cells expressing either wild-type Mad1, or Mad1^{3EK} (the latter to prevent Mad1 and Mad2 corona localization). Cells expressing Spindly^{ACCS} are unable to recruit dynein to kinetochores, but are competent for corona expansion (Gassmann et al., 2010; Sacristan et al., 2018). We measured the mitotic index of each as a readout of checkpoint function. While cells expressing Spindly ACCS and wild-type Mad1 exhibited a mitotic index of 63.9% (Figure 7A), indicative of a robust mitotic arrest, those expressing Spindly^{ACCS} and Mad1^{3EK} had a significantly lower mitotic index (30.8%), suggesting that the absence of checkpoint signaling molecules at the corona permits cells to overcome the lack of kinetochore-associated

To explore this further, we performed time-lapse imaging of these cells and measured their mitotic duration. As shown in Figure 7B, cells expressing wild-type Spindly, irrespective of Mad1 and Mad2 localization to the corona, exited mitosis with normal timing. Consistent with the importance of kinetochore dynein in checkpoint silencing (Gassmann et al., 2010), cells expressing Spindly^{ACCS} and wild-type Mad1 exhibited a robust mitotic arrest, with only a small fraction of cells (8%) exiting mitosis over the course of imaging (15 h). However, the fraction of Spindly^{ΔCCS} and Mad1^{3EK}-expressing cells that exited mitosis during the imaging period was significantly greater (49%; Figure 7B). Although we cannot rule out that these cells exit mitosis due to slightly weaker checkpoint function (as shown in Figure 6, B and E; Allan et al., 2020), taken together with our other data, these findings strongly suggest that dynein's function in silencing the SAC is primarily to remove checkpoint effectors from the fibrous corona. These observations also explain previous results which found that depletion of Spindly, which prevents both

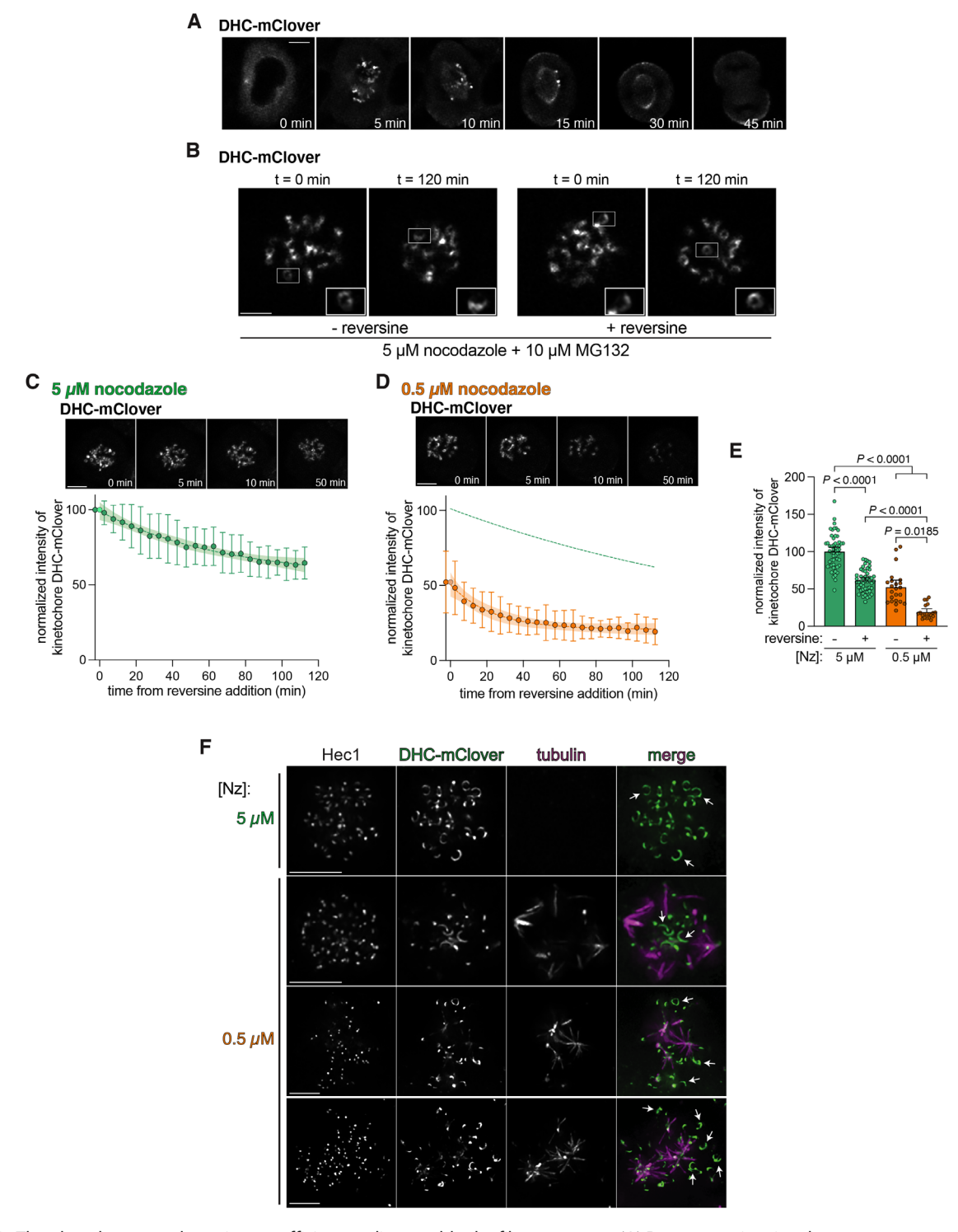


FIGURE 5. The phosphatase pathway is not sufficient to disassemble the fibrous corona. (A) Representative time-lapse fluorescence images of CRISPR/Cas9 DHC-mClover cells progressing through mitosis. Scale bar = $10 \, \mu m$. (B) Representative time-lapse fluorescence images of DHC-mClover cells treated with 5 μm nocodazole overnight and then imaged for 2 h in the absence (left) or presence of $10 \, \mu m$ reversine for 2 h (right). MG132 ($10 \, \mu m$) was included to prevent mitotic exit. Note the distinct corona morphology for DHC-mClover remains even after 2 h in reversine, suggesting that reversine reduces levels of kinetochore dynein, but does not trigger disassembly of the corona. Scale bar = $5 \, \mu m$. (C, D) Representative time-lapse fluorescence images and quantitation of relative DHC-mClover levels in HeLa cells arrested in either (C) $5 \, \mu m$ or (D) $0.5 \, \mu m$ nocodazole (both with $10 \, \mu m$ MG132), and then treated with $10 \, \mu m$ reversine (at time = $0 \, min$). Intensity values were corrected for photobleaching as described in *Materials and Methods* ($n = 51 \, cells$ from $5 \, replicates$ for $5 \, \mu m$; 24 cells from $2 \, replicates$ for $0.5 \, \mu m$). The data (means $\pm 5 \, m$) were fit (green or orange dashed lines; overlaid with 95% confidence interval indicated with shaded green or orange) to one-phase exponential decays with of $t_{1/2}^{5 \, \mu m} = 47.8 \, m$ min and $t_{1/2}^{0.5 \, \mu m} = 15.9 \, m$ in. To account for the time lag between acquiring the prereversine image and the first postreversine image (~2.5 min), we assumed the intensity values for the $0 \, t$ time point for

corona formation and recruitment of dynein to kinetochores, does not preclude SAC silencing (Chan et al., 2009; Gassmann et al., 2010).

We noted that although expression of Spindly $^{\Delta CCS}$ and Mad1 3EK enabled cells to exit mitosis to a greater extent than those expressing Spindly^{ACCS} and wild-type Mad1, they did not reach the same degree of mitotic exit as wild-type cells. To investigate the potential cause for this discrepancy, we expressed histone H2B-mCherry (to label chromosomes) in these cells, and performed time-lapse imaging to monitor mitotic progression and chromosome alignment. This revealed that cells expressing Spindly^{ACCS}, either with wild-type Mad1 or with Mad1^{3EK}, exhibited significant delays in aligning their chromosomes (Figure 7C), thus likely explaining their overall mitotic delay. These data are consistent with a role for kinetochore dynein in chromosome alignment (Varma et al., 2008).

DISCUSSION

Although dynein has been shown to be a critical effector of checkpoint silencing, its precise role in this process has remained elusive. Here we find that dynein's role in silencing the spindle assembly checkpoint is to specifically remove checkpoint effectors (e.g., Mad1 and Mad2) from the fibrous corona, and not the outer kinetochore (Figure 8). This model is based on several findings presented here, including the following: 1) microtubules, and thus the dynein pathway, are required for the reversine-initiated eviction of a population of kinetochore Mad2; 2) the phosphatase pathway is sufficient to initiate complete removal of kinetochore Mad2 in cells lacking corona-localized checkpoint effectors (e.g., those depleted for Spindly, Rod^{2A} cells, or Mad1^{3EK} cells); 3) Rod, a kinetochore-localized dynein cargo, accumulates at spindle poles to a much lesser extent in cells lacking Rod from coronas, suggesting that dynein does not transport outer kinetochore-localized checkpoint effectors to the poles; 4) the phosphatase pathway is not sufficient to remove dynein, Mad2, or RZZ from the fibrous corona (Sacristan et al., 2018); and 5) dynein function in checkpoint silencing becomes largely dispensable in cells lacking corona-localized checkpoint effectors. For this model to be true, it would require that the corona-localized pool of checkpoint effector molecules be capable of eliciting a checkpoint arrest, which we find is also the case. Interestingly, this population of SAC effectors is not absolutely required for checkpoint function, but becomes important in situations in which a small number of chromosomes are misaligned. Our findings also resolve a longstanding mystery in the field: why does depletion of Spindly compromise checkpoint function, whereas a Spindly mutant that is simply defective for dynein-dynactin recruitment maintains a strong checkpoint arrest? Our data indicate the reason for this discrepancy is simply that depletion of Spindly not only prevents dynein recruitment to kinetochores, but also severely compromises corona expansion, thus obviating the need for dynein in SAC silencing.

In light of dynein's reliance on dynactin and a cargo adaptor (e.g., Spindly) for activity (McKenney et al., 2014; Schlager et al., 2014), and that dynein localization to kinetochores requires Spindly and dynactin (Gassmann et al., 2010; Raaijmakers et al., 2013), it seems likely that dynein becomes active for motility simply as a consequence of its recruitment to this site. This raises the question of whether dynein requires additional signals to initiate eviction of kinetochore-localized SAC effectors. Although a previous study suggested that stable end-on attachments are required to trigger kinetochore dynein activity (Kuhn and Dumont, 2017), our work indicates that a subset of kinetochore dynein motors simply respond to the presence of a microtubule. This is also supported by previously published data demonstrating that dynein and its kinetochore cargoes are largely removed shortly after nuclear envelope breakdown, long before establishment of stable kinetochore-microtubule attachments (King et al., 2000; Howell et al., 2001). Thus, unlike outer kinetochore-localized checkpoint effectors that require stable end-on attachments to trigger their complete removal, dynein neither senses nor responds to attachment status per se. Rather, we posit that dynein's role is to prime the kinetochore for checkpoint silencing by removing corona-associated SAC effectors, such that upon establishment of stable end-on attachments, the rapid phosphatase-mediated eviction of the outer kinetochore-localized pool of SAC effectors quickly results in mitotic exit.

Our findings raise an interesting question regarding the potential coevolution of kinetochore dynein with the fibrous corona. It is well established that some organisms with fibrous coronas indeed possess kinetochore dynein (e.g., humans, Xenopus laevis, Caenorhabditis elegans, Drosophila melanogaster, Potorous tridactylus; Cassimeris et al., 1990; Pfarr et al., 1990; Howell et al., 2001; Basto et al., 2004; Stear and Roth, 2004; Cane et al., 2013; Wynne and Funabiki, 2015; Pereira et al., 2018); however, a smaller number of organisms that are known to employ cytoplasmic dynein-1 (e.g., Saccharomyces cerevisiae, Schizosaccharomyces pombe) do not localize this motor to kinetochores. These same organisms also appear to lack coronas, suggesting that these two phenomena are potentially interrelated. In support of a coevolutionary relationship, the molecules responsible for recruiting dynein to the kinetochore are also responsible for corona expansion. In addition to Spindly, expansion of the fibrous corona relies on the upstream recruitment complex RZZ. Although this provides a likely molecular basis for the entwined development of these two phenomena, we can only speculate as to the physiological necessity of the corona. Those organisms with fibrous coronas may rely on them for their chromosome capture function (via microtubule-binding proteins localized to this structure), and/or to signal a checkpoint arrest in situations in which one or two chromosomes are unaligned, both of which reduce the likelihood of chromosome segregation errors. Budding yeast in particular may not require these corona functions due to the fact that their kinetochores are attached to spindle microtubules during most of the cell cycle, including G1 and M phases (Guacci et al., 1997; Jin et al., 2000; Winey and O'Toole, 2001; Tanaka et al., 2002), and thus have a low probability of misalignment. Alternatively, the smaller cell/nuclear size of yeasts compared with metazoa, and the consequent smaller distance between potentially misaligned chromosomes and the mitotic spindle might also obviate the need for these corona functions.

Taken together, our data support the following model for eviction of SAC effectors from kinetochores (Figure 8). In early mitosis,

each were equal to that of the prereversine addition time point (dashed light-green or orange circle). Scale bars = $10~\mu m$. (E) Plots (mean \pm SD) depicting mean normalized intensity for DHC-mClover at the beginning and end of the imaging period. (F) Representative images of DHC-mClover-expressing cells treated with either 5 or 0.5 µM nocodazole overnight. Note the lack of corona-like morphology for those kinetochores that are in close proximity of a microtubule tuft. Statistical significance in panel E was determined by comparing means using a Kruskal-Wallis one-way ANOVA test.

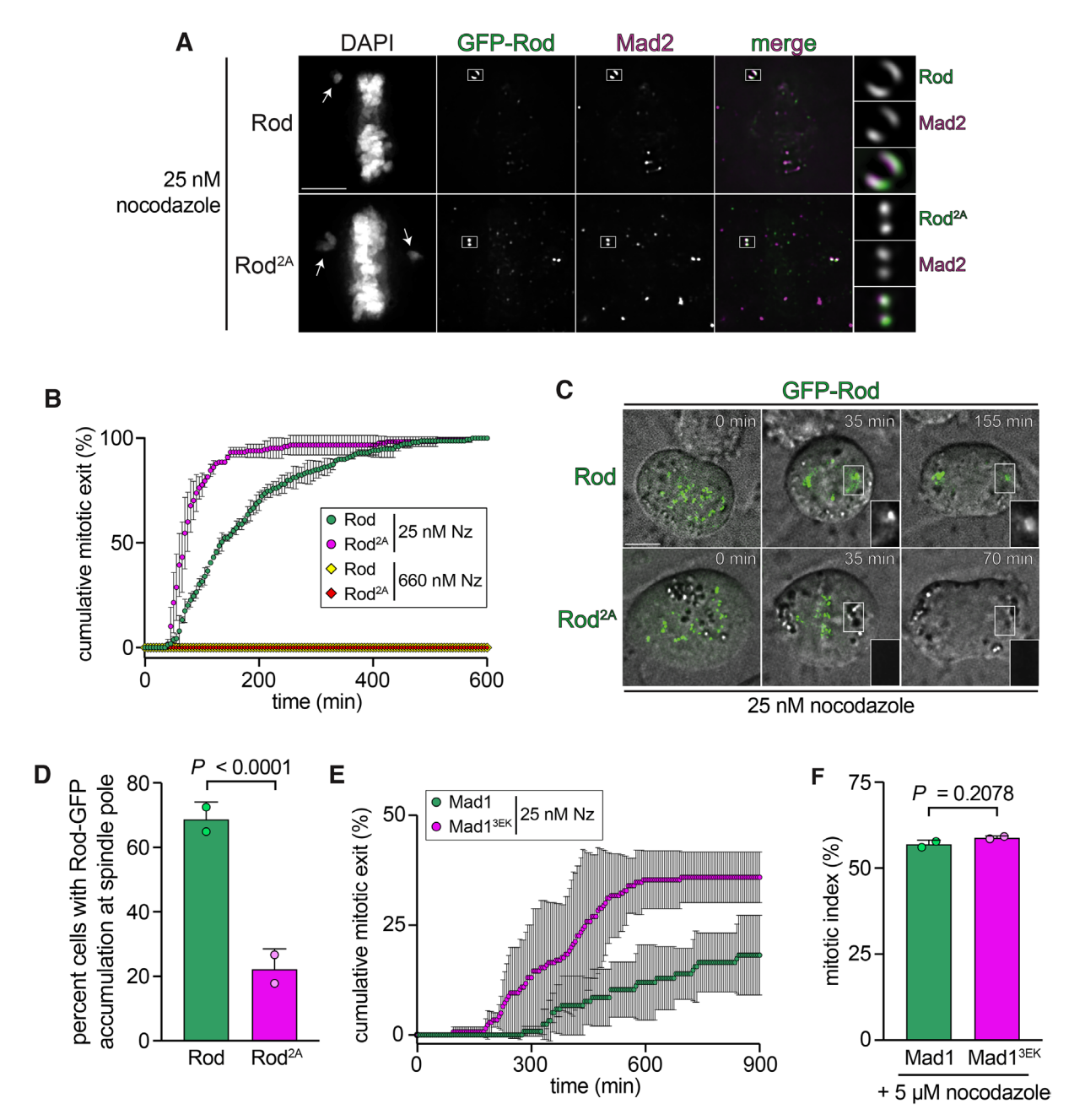


FIGURE 6: Corona-localized Mad2 is required for robust checkpoint signaling. (A) Representative fluorescence images of cells expressing either wild-type Rod, or Rod^{2A} that were treated with 25 nM nocodazole for 2 h, then processed for immunofluorescence. White arrows depict unaligned chromosomes; white boxes delineate one pair of unattached kinetochores with either expanded coronas (in wild-type cells), or not (in Rod^{2A} cells). Scale bar = 10 µm. (B) Plot (mean \pm SD) depicting cumulative mitotic exit (i.e., as a measure of mitotic duration) for cells treated with indicated concentration of nocodazole (treated for 2 h before imaging), and expressing either wild-type GFP-Rod, or GFP-Rod^{2A} (n = 158 cells from 2 replicates for wild-type Rod, 25 nM nocodazole; 140 cells from 2 replicates for Rod^{2A}, 25 nM nocodazole; 86 cells from 2 replicates for wild-type Rod, 660 nM nocodazole; 65 cells from 2 replicates for Rod^{2A}, 660 nM nocodazole). Note the reduced mitotic duration in 25 nM nocodazole-treated cells expressing the Rod^{2A} compared with wild-type Rod, indicating a weakened mitotic checkpoint for cells compromised for corona expansion. (C) Representative still images (fluorescence and DIC) from a time-lapse acquisition of cells for those described in panel B. Scale bar = 10μm. Inset depicts the localization of wild-type Rod to spindle poles, but not Rod^{2A} (GFP channel only). (D) Plot (weighted mean ± weighted standard error of proportion) depicting fraction of cells with wild-type or mutant Rod at spindle poles (as determined from time-lapse images, as described in panel C). (E) Plot (mean \pm SD) depicting cumulative mitotic exit for cells expressing either wild-type Mad1, or Mad1 3EK treated with 25 nM nocodazole for 2 h before imaging (n = 112) cells from 2 replicates for wild-type Mad1; 153 cells from 2 replicates for Mad1^{3EK}). (F) Plot (mean ± SD) depicting mitotic indices of cells expressing either wild-type Mad1 or Mad1 3EK treated with 5 μ M nocodazole for 16 h before being processed for immunofluorescence (n = 2000 cells from 2 replicates for wild-type Mad1; 2109 cells from 2 replicates for Mad1^{3EK}). Note endogenous Mad1 is lacking from these cells (see Materials and Methods). Statistical significance was determined by calculating P values from Z scores for proportion data for panels D and F.

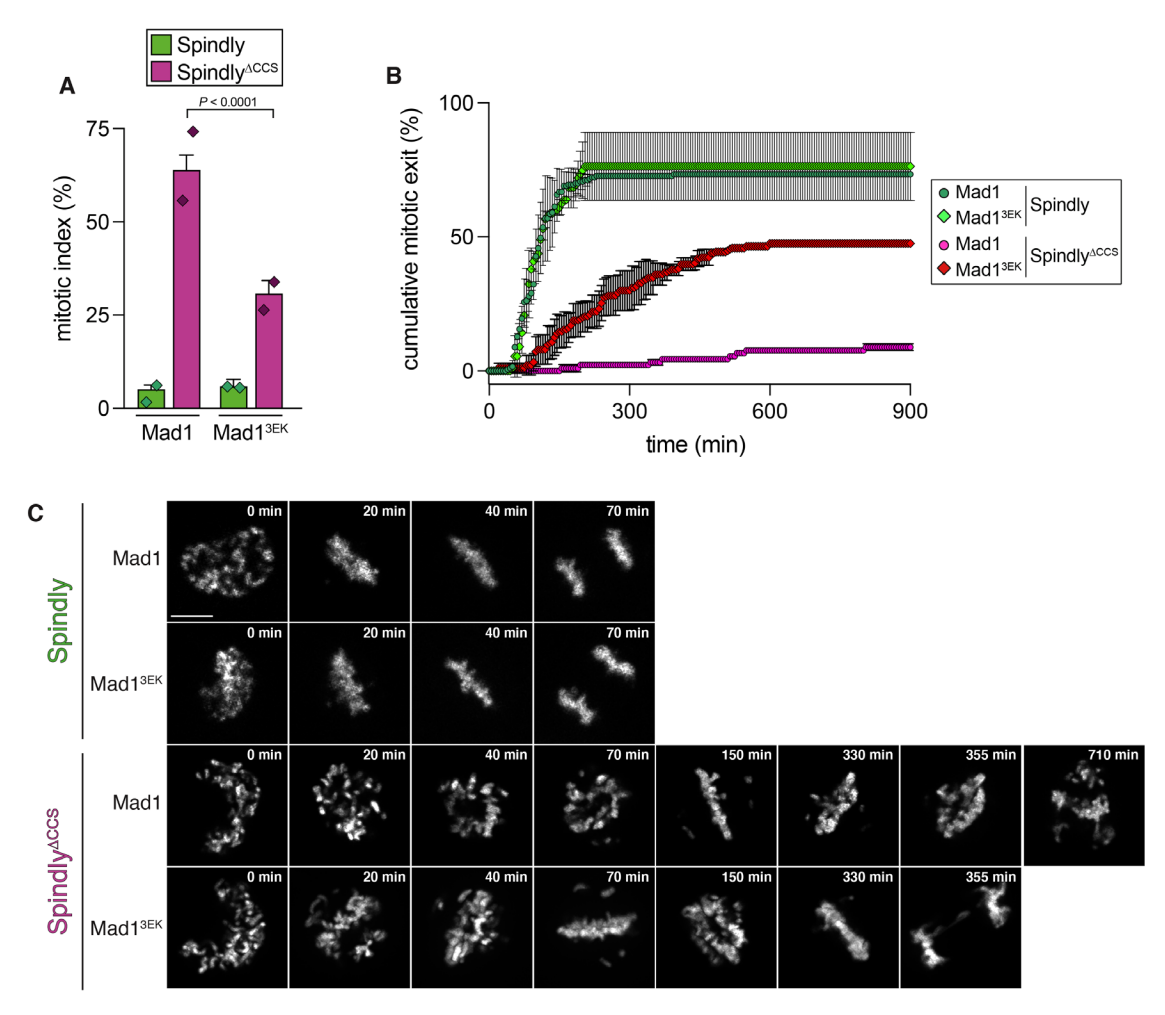


FIGURE 7: Role of kinetochore dynein in checkpoint silencing is restricted to removal of SAC effectors from the corona. (A) Plot (mean ± standard error of proportion) depicting mitotic indices of cells expressing the indicated Spindly (wild-type or Spindly^{ACCS}; note endogenous Spindly was depleted via RNAi) and Mad1 (wild-type or Mad1^{3EK}; endogenous Mad1 was knocked out via CRISPR/Cas9). Note the reduced mitotic index of cells expressing both Spindly^{ACCS} and Mad1^{3EK}, indicating the lack of corona-localized Mad1/Mad2 can compensate for the lack of kinetochore dynein (n = 550 cells from 2 replicates for wild-type Spindly and wild-type Mad1; 305 cells from 2 replicates for wild-type Spindly and Mad1^{3EK}; 280 cells from 2 replicates for Spindly^{ACCS} and wild-type Mad1; 344 cells from 2 replicates for Spindly $^{\Delta CCS}$ and Mad1 3EK). (B) Plot (mean \pm SD) depicting cumulative mitotic exit for cells expressing the indicated Spindly (wild-type or Spindly^{ACCS}) and Mad1 (wild-type or Mad1^{3EK}). As in panel B, note the ability of cells expressing Spindly $^{\Delta CCS}$ and Mad1 3EK to progress through mitosis (compare to cells expressing Spindly $^{\Delta CCS}$ and wild-type Mad1); n = 1114 cells from 2 replicates for wild-type Spindly and wild-type Mad1; 80 cells from 2 replicates for wild-type Spindly and Mad1^{3EK}; 91 cells from 2 replicates for Spindly^{ΔCCS} and wild-type Mad1; 171 cells from 3 replicates for Spindly^{ΔCCS} and Mad1^{3EK}. (C) Representative fluorescence time-lapse images of cells expressing H2B-mCherry, and the indicated Spindly (wild-type or Spindly^{ΔCCS}) and Mad1 (wild-type or Mad1^{3EK}). Scale bar = 10 μm. Statistical significance was determined by calculating P values from Z scores for proportion data for panel A.

kinetochores begin to make attachments to spindle microtubules, likely aided in part by corona-localized attachment factors (e.g., CENP-E, dynein) that promote chromosome congression and alignment. Our data indicate that transient (e.g., lateral) kinetochore-microtubule encounters early in mitosis lead to dynein-mediated eviction of corona-localized SAC effectors (Figure 8Aii). This early dynein-mediated activity helps to prime the kinetochores and thus the checkpoint for rapid silencing upon proper alignment and attachment of all the chromosomes (Figure 8Aiii). Our findings indicate that those chromosomes that are distal from the spindle that retain their coronas due to a lack of microtubule attachment are sufficient to prevent anaphase onset due to the generation of active

MCCs from them (even in the presence of a small number of such misaligned chromosomes). Thus, an expanded corona provides cells with a critical tool in the prevention of chromosome misalignment, and the consequent development of aneuploidy.

MATERIALS AND METHODS

Request a protocol through Bio-protocol.

Cell culture

All cell lines used in this article were cultured in DMEM supplemented with 10% fetal bovine serum (FBS), 1% antibiotic/antimycotic solution, and 4 mM L-glutamine and maintained at 37°C in 5%

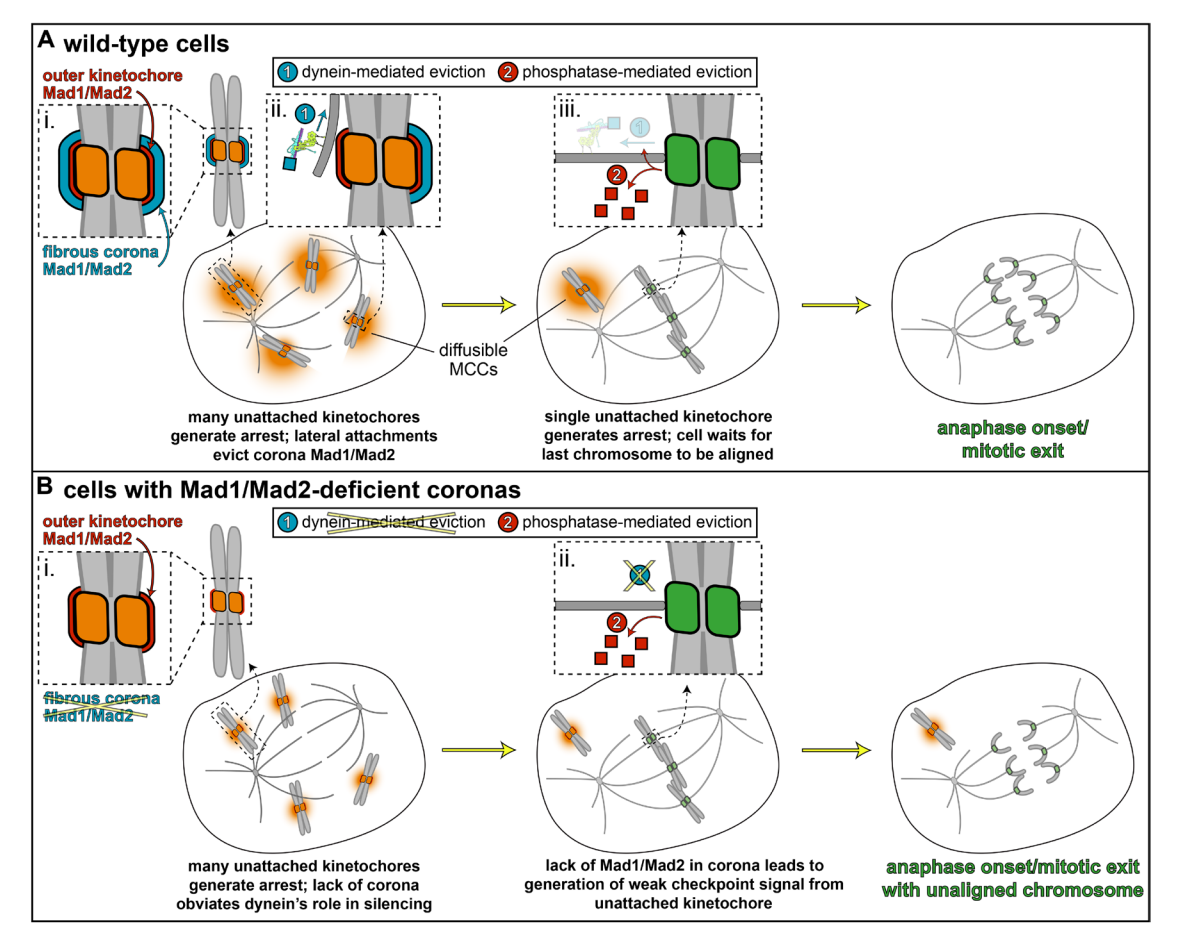


FIGURE 8: Model for dynein and the corona in spindle assembly checkpoint function. In wild-type cells (A) or in cells without Mad1/Mad2 at the fibrous corona (B; see Bi), a large number of unattached kinetochores in early mitosis can generate a sufficiently strong "wait anaphase" signal (comprised of diffusible MCC complexes; see orange gradient) that arrests mitotic progression. In early mitosis, as kinetochores make transient (e.g., lateral) microtubule attachments (see Aii), dynein evicts corona-localized Mad1 and Mad2 (blue square in Aii) in an indiscriminate manner. By specifically removing these molecules, dynein primes the kinetochore for rapid phosphatase-mediated eviction that is triggered by establishment of a stable, end-on attachment (see Aiii). Given that dynein performs this priming function early in prometaphase, the role of dynein in removing SAC effectors during late prometaphase is likely minimal. Unlike the dynein pathway, the phosphatase-mediated eviction of SAC effectors (see red squares in Aiii and Bii) is directly triggered by attachment status. Without corona-localized Mad1/Mad2, dynein function in checkpoint silencing becomes dispensable, and likely transports no SAC effectors (see Bii). The checkpoint function of the corona-localized pool of Mad1/Mad2 becomes especially apparent in situations in which a small number of chromosomes are unaligned. Without these molecules, cells likely exit mitosis with unaligned chromosomes.

CO₂. Doxycycline-inducible vsv-Mad1^{WT} and vsv-Mad1^{3EK} HeLa cell lines (a gift from Lindsay Allan and Adrian Saurin, University of Dundee, Dundee, UK) were continuously cultured with 1 µg/ml doxycycline (Sigma Aldrich) to maintain expression of Mad1 transgenes. Note these cells are lacking endogenous Mad1 due to CRISPR/Cas9-mediated knockout (Allan et al., 2020). Doxycycline-inducible HeLa FlpIn T-Rex LAP-Rod^{WT} and Rod^{2A} cell lines were a gift from Prasad Jallepalli (Sloan Kettering Institute, New York, NY).

Cell treatments and transfections

For fixed-cell analysis, cells were grown on sterile, acid-washed coverslips in six-well plates. All nucleic acid transfections were done in Optimem (Life Technologies). 100 nM Rod siRNA (5'-TTGTA-CAATCTCTGTATTATA-3') was transfected into cells using Oligofectamine (Fisher Scientific), or 100 nM Spindly siRNA (5'-GAAAGG-GUCUCAAACUGAA-3'; Gassmann et al., 2010) was transfected into cells using Lipofectamine 3000 (Fisher Scientific), both accord-

ing to the manufacturer's protocol. Cells treated with Spindly siRNA were processed for immunofluorescence or live-cell imaging 48 h after addition of siRNA, while those treated with Rod siRNA were processed after 60 h. Plasmids encoding the following constructs were transfected into cells at the indicated concentrations using Lipofectamine 3000 according to the manufacturer's protocol: Mad2-GFP, 1 μg; BubR1-GFP, 1 μg; cyclin-B1-mCherry, 0.75 μg; Spindly^{WT}-GFP, 1.5 μg; Spindly^{ΔCCS}-GFP, 0.5 μg; H2B-mCherry, 0.75 µg. Cells transfected with BubR1-GFP and cyclinB1-mCherry were processed for immunofluorescence or live-cell imaging 24 h after transfection; cells transfected with Mad2-GFP, SpindlyWT-GFP, Spindly^{△CCS}-GFP, or H2B-mCherry were processed after 48 h. For experiments involving HeLa FlpIn T-Rex LAP-RodWT and Rod2A cell lines, cells were transfected with Rod siRNA, and then transgene expression was induced 48 h later using 1 µg/ml doxycycline. Cells were processed for imaging 16 h later. For live-cell reversine eviction assays, cells were incubated with either 5 μM or 0.5 μM

nocodazole (Tocris Bioscience) for 16 h before imaging (see text). Immediately before imaging, cells were washed into a solution containing the appropriate concentration of nocodazole, 10 µM MG-132 (Selleckchem; to prevent anaphase onset), and a 1:100 dilution of OxyFluor (Oxyrase) to minimize the effects of photobleaching during imaging. Live-cell images were collected on a spinningdisk confocal microscope (described below). Immediately after the first time point, 10 µM reversine (Adoog Bioscience) was added to the dish, after which cells continued to be imaged (every 5 min) for 2 h. To control for photobleaching, a second dish was imaged using identical conditions (e.g., laser power, exposure), except without the addition of reversine. For fixed-cell reversine eviction assays, cells were incubated with either 5 μM or 0.5 μM nocodazole (see text) for 16–18 h before being processed for immunofluorescence. After incubating in nocodazole for 16 h, control cells were fixed, and experimental cells were washed into a solution containing the appropriate concentration of nocodazole, 10 µM MG-132, and $10 \, \mu M$ reversine, incubated for 2 h, and then fixed and processed. For characterization of mitotic timing of HeLa FlpIn T-Rex LAP-Rod^{WT} and Rod^{2A} cell lines, and doxycycline-inducible vsv-Mad1^{WT} and Mad1^{3EK} HeLa cell lines in nocodazole, cells were treated with the indicated concentration of nocodazole (see text) for 2 h before being processed for imaging.

Generation of DHC-mClover CRISPR cell line

Single-guide RNAs (sgRNAs) targeting the C-terminal exon of human DYNC1H1 were designed using CCTop (Stemmer et al., 2015). Guide RNAs were cloned into the plasmid pX330-U6-Chimeric_BB-CBh-hSpCas9 (Addgene plasmid 42230; Cong et al., 2013) using procedures as described (Bauer et al., 2015). Homology-directed repair donor plasmids were generated by combining DNA sequences corresponding to approximately 200 base pairs homology arms from the 3' end of DYNC1H1 and mAID-mClover-Hygro^R from plasmid pMK290 (Addgene plasmid 72828), as previously described (Natsume et al., 2016). Twenty-four hours before transfection, 1.5×10^5 HeLa Kyoto cells were plated in one well of a six-well plate. CRISPR/Cas9 plasmid (2 µg; pX330 plasmid described above, encoding gRNA and SpCas9) and 2 µg of the donor plasmid (encoding mAID-mClover-Hygro^R flanked by DYNC1H1 homology arms) were cotransfected into HeLa Kyoto cells using Lipofectamine 3000 according to the manufacturer's instructions. Forty-eight hours following transfection, selection medium was added to the cells (DMEM containing 300 µg/ml hygromycin) to select for positive clones. The selection medium was exchanged every 3 to 4 d. After 10 to 12 d, colonies were transferred to a 24-well plate. Clones were screened for mClover expression using fluorescence microscopy. Optimally expressing clones were frozen down for later use.

Immunofluorescence

Cells were rinsed in 37°C PHEM buffer (60 mM PIPES, 25 mM HEPES, 10 mM EGTA, and 4 mM MgSO $_4$, pH 7.0) and then lysed by incubation for 3 min in freshly prepared lysis buffer (PHEM buffer + 0.5% Triton X-100). Cells were subsequently fixed for 20 min at room temperature in freshly prepared 4% paraformaldehyde in PHEM buffer (37°C). After fixation, cells were washed three times, 5 min each, in PHEM-T (PHEM buffer + 0.1% Triton X-100) and blocked in 10% boiled donkey serum (BDS) in PHEM buffer for 1 h at room temperature. Primary antibodies (including recombinant antibodies generated in-house; DeLuca et al., 2021) were diluted in 5% BDS and added to coverslips overnight at 4°C. See Supplemental Table S1 for primary antibody information. After incubation with

primary antibody, cells were rinsed three times, 5 min each, in PHEM-T and then incubated for 45 min at room temperature with secondary antibodies conjugated to Alexa 488, Cy3, or Alexa 647 (Jackson ImmunoResearch Laboratories) at 1:600 diluted in 5% BDS. Cells were rinsed three times, 5 min each, in PHEM-T and quickly rinsed in PHEM followed by incubation in DAPI (2 ng/ml) diluted in PHEM for 30 s. Cells were rinsed three times, 5 min each, in PHEM-T, quickly rinsed in PHEM, and then mounted onto glass slides with antifade solution (90% glycerol, 0.5% N-propyl gallate). Coverslips were sealed with nail polish and stored at 4°C.

Anti-Spindly antibody production

Antibodies against full-length Spindly were generated at Rockland Immunochemicals (Limerick, PA). Rabbits were immunized with protein purified from bacteria containing pGEX6P1:Spindly (a gift from Reto Gassman, Universidade do Porto, Porto, Portugal). Briefly, bacteria were lysed by sonication in lysis buffer (phosphate-buffered saline [PBS] supplemented with 10 mM EGTA, 10 mM EDTA, 0.1% Tween-20, 250 mM NaCl, 1 mM PMSF, and 2 mM benzamidine-HCl). The clarified lysate was incubated with glutathione agarose for 1 h, which was subsequently washed four times with wash buffer (PBS supplemented with 0.1% Tween-20, 250 mM NaCl, and 1 mM DTT). Bound protein was eluted with elution buffer (50 mM Tris, 75 mM KCl, and 10 mM glutathione, pH 8.1), assessed by SDS-PAGE, and used for immunization (approximate concentration = 0.7 mg/ml). Anti-Spindly antibody was affinity purified from rabbit plasma using bacterially expressed GST-Spindly.

Imaging and fluorescence quantification

All fixed-cell images were acquired on an Inverted Olympus microscope incorporated into a GE Ultra imaging system (GE Healthcare) with SoftWoRx software (GE Healthcare) using a 60x, 1.42 NA differential interference contrast Plan Apochromat oil immersion lens (Olympus) with a final magnification of 107.6 nm/pixel at the camera sensor (edge4.2; PCO). For live-cell imaging experiments, cells were imaged in 35-mm glass-bottomed dishes (MatTek Corporation) and imaged in Leibovitz's I-15 media (Invitrogen) supplemented with 10% FBS, 7 mM HEPES, 4.5 g/l glucose, pH 7.0. Livecell images were captured on a Nikon Ti-E microscope equipped with a Piezo Z-control (Physik Instrumente), stage top incubation system (Okolab), and spinning-disk confocal scanner unit (CSUX1; Yokogawa), using a 60×, 1.49 NA objective and an iXon DU888 EM-CCD camera (Andor). For live-cell reversine eviction assays, three z planes at 1.25 µm steps were acquired every 5 min for 2 h using the 488 or 555 nm lasers. For experiments characterizing mitotic timing in live cells, z stacks were acquired taking three to five z planes for a range of 4–6 µm every 5 min for 15 h using 488 and 594 nm lasers and/or transmitted light. For quantification of kinetochore fluorescence intensities in fixed cells, measurements were performed on nondeconvolved, uncompressed images using the custom "SpeckleTracker" MatLab (MathWorks) program (Wan et al., 2009). For quantification of fluorescence intensities in live cells, backgroundcorrected values were measured from maximum intensity projections using NIS Elements (Nikon). A circular region of interest (ROI) circumscribing the kinetochores was drawn in a nocodazole-treated cell, and the total integrated intensity and area of the circle were logged. Background fluorescence levels were determined by drawing multiple smaller circular ROIs outside of the region of kinetochore fluorescence. For mitotic index and timing experiments (Figure 7, B and C), those cells with average pixel values of 500-1500 A.U. (for Spindly-GFP or Spindly^{△CCS}-GFP) in prophase nuclei were assessed.

ACKNOWLEDGMENTS

We are grateful to Tyler Biebighauser, Jenna Kelly, and Jeanne Mick for technical assistance, Prasad V. Jallepalli (Sloan Kettering Institute, New York, NY) for sharing the wild-type GFP-Rod and GFP-Rod^{2A}-expressing stable cell lines, Lindsey Allan and Adrian Saurin (University of Dundee, Dundee, UK) for providing the stable Mad1 and Mad1^{3EK}-expressing cell lines, and Reto Gassman (Universidade do Porto, Porto, Portugal) for the bacterial GST-Spindly expression plasmid. This work was funded by the National Science Foundation (Grant no. NSF-2107444 to S.M.M. and J.G.D.).

REFERENCES

- Agarwal S, Varma D (2015). How the SAC gets the axe: integrating kinetochore microtubule attachments with spindle assembly checkpoint signaling. Bioarchitecture 5, 1–12.
- Alfieri C, Chang L, Zhang Z, Yang J, Maslen S, Skehel M, Barford D (2016). Molecular basis of APC/C regulation by the spindle assembly check-point. Nature 536, 431–436.
- Alfieri C, Zhang S, Barford D (2017). Visualizing the complex functions and mechanisms of the anaphase promoting complex/cyclosome (APC/C). Open Biol 7, 170204.
- Allan LA, Camacho Reis M, Ciossani G, Huis In 't Veld PJ, Wohlgemuth S, Kops GJ, Musacchio A, Saurin AT (2020). Cyclin B1 scaffolds MAD1 at the kineto-chore corona to activate the mitotic checkpoint. EMBO J 39, e103180.
- Bader JR, Vaughan KT (2010). Dynein at the kinetochore: timing, interactions and functions. Semin Cell Dev Biol 21, 269–275.
- Ballister ER, Riegman M, Lampson MA (2014). Recruitment of Mad1 to metaphase kinetochores is sufficient to reactivate the mitotic checkpoint. J Cell Biol 204, 901–908.
- Barisic M, Sohm B, Mikolcevic P, Wandke C, Rauch V, Ringer T, Hess M, Bonn G, Geley S (2010). Spindly/CCDC99 is required for efficient chromosome congression and mitotic checkpoint regulation. Mol Biol Cell 21, 1968–1981.
- Basto R, Scaerou F, Mische S, Wojcik E, Lefebvre C, Gomes R, Hays T, Karess R (2004). In vivo dynamics of the rough deal checkpoint protein during *Drosophila* mitosis. Curr Biol 14, 56–61.
- Bauer DE, Canver MC, Orkin SH (2015). Generation of genomic deletions in mammalian cell lines via CRISPR/Cas9. J Vis Exp (95), e52118.
- Brady DM, Hardwick K.G (2000). Complex formation between Mad1p, Bub1p and Bub3p is crucial for spindle checkpoint function. Curr Biol 10, 675–678.
- Buffin E, Lefebvre C, Huang J, Gagou ME, Karess RE (2005). Recruitment of Mad2 to the kinetochore requires the Rod/Zw10 complex. Curr Biol 15, 856–861.
- Cane S, McGilvray PT, Maresca TJ (2013). Insights from an erroneous kinetochore-microtubule attachment state. Bioarchitecture 3, 69–76.
- Cassimeris L, Rieder CL, Rupp G, Salmon ED (1990). Stability of microtubule attachment to metaphase kinetochores in PtK1 cells. J Cell Sci 96 (Pt 1): 9–15.
- Chan YW, Fava LL, Uldschmid A, Schmitz MH, Gerlich DW, Nigg EA, Santamaria A (2009). Mitotic control of kinetochore-associated dynein and spindle orientation by human Spindly. J Cell Biol 185, 859–874.
- Chan GK, Jablonski SA, Starr DA, Goldberg ML, Yen TJ (2000). Human Zw10 and ROD are mitotic checkpoint proteins that bind to kinetochores. Nat Cell Biol 2, 944–947.
- Chang L, Zhang Z, Yang J, McLaughlin SH, Barford D (2015). Atomic structure of the APC/C and its mechanism of protein ubiquitination. Nature 522, 450–454.
- Chao WC, Kulkarni K, Zhang Z, Kong EH, Barford D (2012). Structure of the mitotic checkpoint complex. Nature 484, 208–213.
- Chen RH, Shevchenko A, Mann M, Murray AW (1998). Spindle checkpoint protein Xmad1 recruits Xmad2 to unattached kinetochores. J Cell Biol 143, 283–295.
- Cong L, Ran FA, Cox D, Lin S, Barretto R, Habib N, Hsu PD, Wu X, Jiang W, Marraffini LA, Zhang F (2013). Multiplex genome engineering using CRISPR/Cas systems. Science 339, 819–823.
- d'Amico EA, Ud Din Ahmad M, Cmentowski V, Girbig M, Muller F, Wohlgemuth S, Brockmeyer A, Maffini S, Janning P, Vetter IR, et al. (2022). Conformational transitions of the Spindly adaptor underlie its interaction with Dynein and Dynactin. J Cell Biol 221, e202206131.
- De Antoni A, Pearson CG, Cimini D, Canman JC, Sala V, Nezi L, Mapelli M, Sironi L, Faretta M, Salmon ED, Musacchio A (2005). The Mad1/Mad2 complex as a template for Mad2 activation in the spindle assembly checkpoint. Curr Biol 15, 214–225.

- DeLuca JG, Howell BJ, Canman JC, Hickey JM, Fang G, Salmon ED (2003). Nuf2 and Hec1 are required for retention of the checkpoint proteins Mad1 and Mad2 to kinetochores. Curr Biol 13, 2103–2109.
- DeLuca KF, Mick JE, Ide AH, Lima WC, Sherman L, Schaller KL, Anderson SM, Zhao N, Stasevich TJ, Varma D, et al. (2021). Generation and diversification of recombinant monoclonal antibodies. eLife 10, 72093.
- Di Fiore B, Wurzenberger C, Davey NE, Pines J (2016). The mitotic checkpoint complex requires an evolutionary conserved cassette to bind and inhibit active APC/C. Mol Cell 64, 1144–1153.
- Etemad B, Kops GJ (2016). Attachment issues: kinetochore transformations and spindle checkpoint silencing. Curr Opin Cell Biol 39, 101–108.
- Etemad B, Kuijt TE, Kops GJ (2015). Kinetochore-microtubule attachment is sufficient to satisfy the human spindle assembly checkpoint. Nat Commun 6, 8987.
- Famulski JK, Vos LJ, Rattner JB, Chan GK (2011). Dynein/dynactin-mediated transport of kinetochore components off kinetochores and onto spindle poles induced by nordihydroguaiaretic acid. PLoS One 6, e16494.
- Firestone AJ, Weinger JS, Maldonado M, Barlan K, Langston LD, O'Donnell M, Gelfand VI, Kapoor TM, Chen JK (2012). Small-molecule inhibitors of the AAA+ ATPase motor cytoplasmic dynein. Nature 484, 125–129.
- Fischer ES, Yu CWH, Bellini D, McLaughlin SH, Orr CM, Wagner A, Freund SMV, Barford D (2021). Molecular mechanism of Mad1 kinetochore targeting by phosphorylated Bub1. EMBO Rep 22, e52242.
- Gama JB, Pereira C, Simoes PA, Celestino R, Reis RM, Barbosa DJ, Pires HR, Carvalho C, Amorim J, Carvalho AX, et al. (2017). Molecular mechanism of dynein recruitment to kinetochores by the Rod-Zw10-Zwilch complex and Spindly. J Cell Biol 216, 943–960.
- Garvanska DH, Nilsson J (2020). Specificity determinants of phosphoprotein phosphatases controlling kinetochore functions. Essays Biochem 64, 325–336.
- Gassmann R, Essex A, Hu JS, Maddox PS, Motegi F, Sugimoto A, O'Rourke SM, Bowerman B, McLeod I, Yates JR 3rd, et al. (2008). A new mechanism controlling kinetochore-microtubule interactions revealed by comparison of two dynein-targeting components: SPDL-1 and the Rod/Zwilch/Zw10 complex. Genes & development 22, 2385–2399.
- Gassmann R, Holland AJ, Varma D, Wan X, Civril F, Cleveland DW, Oegema K, Salmon ED, Desai A (2010). Removal of Spindly from microtubule-attached kinetochores controls spindle checkpoint silencing in human cells. Genes Dev 24, 957–971.
- Gorbsky GJ (2015). The spindle checkpoint and chromosome segregation in meiosis. FEBS J 282, 2471–2487.
- Guacci V, Hogan E, Koshland D (1997). Centromere position in budding yeast: evidence for anaphase A. Mol Biol Cell 8, 957–972.
- Heasley LR, Markus SM, DeLuca JG (2017). "Wait anaphase" signals are not confined to the mitotic spindle. Mol Biol Cell 28, 1186–1194.
- Herzog F, Primorac I, Dube P, Lenart P, Sander B, Mechtler K, Stark H, Peters JM (2009). Structure of the anaphase-promoting complex/cyclosome interacting with a mitotic checkpoint complex. Science 323, 1477–1481
- Hiruma Y, Sacristan C, Pachis ST, Adamopoulos A, Kuijt T, Ubbink M, von Castelmur E, Perrakis A, Kops GJ (2015). CELL DIVISION CYCLE. Competition between MPS1 and microtubules at kinetochores regulates spindle checkpoint signaling. Science 348, 1264–1267.
- Hoffman DB, Pearson CG, Yen TJ, Howell BJ, Salmon ED (2001). Microtubule-dependent changes in assembly of microtubule motor proteins and mitotic spindle checkpoint proteins at PtK1 kinetochores. Mol Biol Cell 12, 1995–2009.
- Howell BJ, McEwen BF, Canman JC, Hoffman DB, Farrar EM, Rieder CL, Salmon ED (2001). Cytoplasmic dynein/dynactin drives kinetochore protein transport to the spindle poles and has a role in mitotic spindle checkpoint inactivation. J Cell Biol 155, 1159–1172.
- Howell BJ, Moree B, Farrar EM, Stewart S, Fang G, Salmon ED (2004). Spindle checkpoint protein dynamics at kinetochores in living cells. Curr Biol 14, 953–964.
- Ji Z, Gao H, Jia L, Li B, Yu H (2017). A sequential multi-target Mps1 phosphorylation cascade promotes spindle checkpoint signaling. eLife 6, 22513.
- Ji Z, Gao H, Yu H (2015). CELL DIVISION CYCLE. Kinetochore attachment sensed by competitive Mps1 and microtubule binding to Ndc80C. Science 348, 1260–1264.
- Jin QW, Fuchs J, Loidl J (2000). Centromere clustering is a major determinant of yeast interphase nuclear organization. J Cell Sci 113 (Pt 11): 1903–1912.
- King JM, Hays TS, Nicklas RB (2000). Dynein is a transient kinetochore component whose binding is regulated by microtubule attachment, not tension. J Cell Biol 151, 739–748.

- Kops G, Gassmann R (2020). Crowning the kinetochore: the fibrous corona in chromosome segregation. Trends Cell Biol 30, 653-667.
- Kops GJ, Kim Y, Weaver BA, Mao Y, McLeod I, Yates JR 3rd, Tagaya M, Cleveland DW (2005). ZW10 links mitotic checkpoint signaling to the structural kinetochore. J Cell Biol 169, 49-60.
- Kops G, Snel B, Tromer EC (2020). Evolutionary dynamics of the spindle assembly checkpoint in eukaryotes. Curr Biol 30, R589-R602.
- Kuhn J, Dumont S (2017). Spindle assembly checkpoint satisfaction occurs via end-on but not lateral attachments under tension. J Cell Biol 216, 1533-1542
- Lara-Gonzalez P, Pines J, Desai A (2021). Spindle assembly checkpoint activation and silencing at kinetochores. Semin Cell Dev Biol 117, 86-98.
- Larsen NA, Al-Bassam J, Wei RR, Harrison SC (2007). Structural analysis of Bub3 interactions in the mitotic spindle checkpoint. Proc Natl Acad Sci USA 104, 1201-1206.
- Lischetti T, Nilsson J (2015). Regulation of mitotic progression by the spindle assembly checkpoint. Mol Cell Oncol 2, e970484.
- London N, Biggins S (2014a). Mad1 kinetochore recruitment by Mps1-mediated phosphorylation of Bub1 signals the spindle checkpoint. Genes Dev 28, 140-152.
- London N, Biggins S (2014b). Signalling dynamics in the spindle checkpoint response. Nat Rev Mol Cell Biol 15, 736-747.
- London N, Ceto S, Ranish JA, Biggins S (2012). Phosphoregulation of Spc105 by Mps1 and PP1 regulates Bub1 localization to kinetochores. Curr Biol 22, 900-906.
- Luo X, Tang Z, Rizo J, Yu H (2002). The Mad2 spindle checkpoint protein undergoes similar major conformational changes upon binding to either Mad1 or Cdc20. Mol Cell 9, 59-71
- Magidson V, O'Connell CB, Loncarek J, Paul R, Mogilner A, Khodjakov A (2011). The spatial arrangement of chromosomes during prometaphase facilitates spindle assembly. Cell 146, 555-567
- Magidson V, Paul R, Yang N, Ault JG, O'Connell CB, Tikhonenko I, McEwen BF, Mogilner A, Khodjakov A (2015). Adaptive changes in the kinetochore architecture facilitate proper spindle assembly. Nat Cell Biol 17, 1134-1144.
- McKenney RJ, Huynh W, Tanenbaum ME, Bhabha G, Vale RD (2014). Activation of cytoplasmic dynein motility by dynactin-cargo adapter complexes. Science 345, 337-341.
- Mosalaganti S, Keller J, Altenfeld A, Winzker M, Rombaut P, Saur M, Petrovic A, Wehenkel A, Wohlgemuth S, Muller F, et al. (2017). Structure of the RZZ complex and molecular basis of its interaction with Spindly. J Cell Biol 216, 961-981.
- Moura M, Conde C (2019). Phosphatases in mitosis: roles and regulation. Biomolecules 9, 55.
- Musacchio A, Desai A (2017). A molecular view of kinetochore assembly and function. Biology (Basel) 6, 5.
- Natsume T, Kiyomitsu T, Saga Y, Kanemaki MT (2016). Rapid protein depletion in human cells by auxin-inducible degron tagging with short homology donors. Cell Rep 15, 210-218.
- Nijenhuis W, Vallardi G, Teixeira A, Kops GJ, Saurin AT (2014). Negative feedback at kinetochores underlies a responsive spindle checkpoint signal. Nat Cell Biol 16, 1257-1264.
- Pereira C, Reis RM, Gama JB, Celestino R, Cheerambathur DK, Carvalho AX, Gassmann R (2018). Self-assembly of the RZZ complex into filaments drives kinetochore expansion in the absence of microtubule attachment. Curr Biol 28, 3408-3421 e3408.
- Pesenti ME, Weir JR, Musacchio A (2016). Progress in the structural and functional characterization of kinetochores. Curr Opin Struct Biol 37, 152-163.
- Pfarr CM, Coue M, Grissom PM, Hays TS, Porter ME, McIntosh JR (1990). Cytoplasmic dynein is localized to kinetochores during mitosis. Nature
- Primorac I, Weir JR, Chiroli E, Gross F, Hoffmann I, van Gerwen S, Ciliberto A, Musacchio A (2013). Bub3 reads phosphorylated MELT repeats to promote spindle assembly checkpoint signaling. eLife 2, e01030.
- Raaijmakers JA, Tanenbaum ME, Medema RH (2013). Systematic dissection of dynein regulators in mitosis. J Cell Biol 201, 201–215.
- Rieder CL (1982). The formation, structure, and composition of the mammalian kinetochore and kinetochore fiber. Int Rev Cytol 79, 1-58.
- Ris H, Witt PL (1981). Structure of the mammalian kinetochore. Chromosoma 82, 153-170.
- Rodriguez-Rodriguez JA, Lewis C, McKinley KL, Sikirzhytski V, Corona J, Maciejowski J, Khodjakov A, Cheeseman IM, Jallepalli PV (2018) Distinct roles of RZZ and Bub1-KNL1 in mitotic checkpoint signaling and kinetochore expansion. Curr Biol 28, 3422-3429 e3425.

- Sacristan C, Ahmad MUD, Keller J, Fermie J, Groenewold V, Tromer E, Fish A, Melero R, Carazo JM, Klumperman J, et al. (2018). Dynamic kinetochore size regulation promotes microtubule capture and chromosome biorientation in mitosis. Nat Cell Biol 20, 800-810.
- Sacristan C, Kops GJ (2015). Joined at the hip: kinetochores, microtubules, and spindle assembly checkpoint signaling. Trends Cell Biol 25, 21-28.
- Santaguida S, Tighe A, D'Alise AM, Taylor SS, Musacchio A (2010). Dissecting the role of MPS1 in chromosome biorientation and the spindle checkpoint through the small molecule inhibitor reversine. J Cell Biol 190, 73-87
- Saurin AT (2018). Kinase and phosphatase cross-talk at the kinetochore. Front Cell Dev Biol 6, 62.
- Schlager MA, Hoang HT, Urnavicius L, Bullock SL, Carter AP (2014). In vitro reconstitution of a highly processive recombinant human dynein complex. EMBO J 33, 1855-1868.
- Shepperd LA, Meadows JC, Sochaj AM, Lancaster TC, Zou J, Buttrick GJ, Rappsilber J, Hardwick KG, Millar JB (2012). Phosphodependent recruitment of Bub1 and Bub3 to Spc7/KNL1 by Mph1 kinase maintains the spindle checkpoint. Curr Biol 22, 891-899
- Silio V, McAinsh AD, Millar JB (2015). KNL1-Bubs and RZZ provide two separable pathways for checkpoint activation at human kinetochores. Dev Cell 35, 600-613.
- Silva PM, Reis RM, Bolanos-Garcia VM, Florindo C, Tavares AA, Bousbaa H (2014). Dynein-dependent transport of spindle assembly checkpoint proteins off kinetochores toward spindle poles. FEBS Lett 588, 3265-3273.
- Sironi L, Mapelli M, Knapp S, De Antoni A, Jeang KT, Musacchio A (2002). Crystal structure of the tetrameric Mad1-Mad2 core complex: implications of a 'safety belt' binding mechanism for the spindle checkpoint. EMBO J 21, 2496-2506
- Stear JH, Roth MB (2004). The Caenorhabditiselegans kinetochore reorganizes at prometaphase and in response to checkpoint stimuli. Mol Biol Cell 15, 5187-5196.
- Stemmer M, Thumberger T, Del Sol Keyer M, Wittbrodt J, Mateo JL (2015). CCTop: an intuitive, flexible and reliable CRISPR/Cas9 target prediction tool. PLoS One 10, e0124633.
- Steuer ER, Wordeman L, Schroer TA, Sheetz MP (1990). Localization of cytoplasmic dynein to mitotic spindles and kinetochores. Nature 345,
- Sudakin V, Chan GK, Yen TJ (2001). Checkpoint inhibition of the APC/C in HeLa cells is mediated by a complex of BUBR1, BUB3, CDC20, and MAD2. J Cell Biol 154, 925-936.
- Tanaka TU, Rachidi N, Janke C, Pereira G, Galova M, Schiebel E, Stark MJ, Nasmyth K (2002). Evidence that the Ipl1-Sli15 (Aurora kinase-INCENP) complex promotes chromosome bi-orientation by altering kinetochorespindle pole connections. Cell 108, 317-329.
- Tauchman EC, Boehm FJ, DeLuca JG (2015). Stable kinetochore-microtubule attachment is sufficient to silence the spindle assembly checkpoint in human cells. Nat Commun 6, 10036.
- Thrower DA, Jordan MA, Wilson L (1996). Modulation of CENP-E organization at kinetochores by spindle microtubule attachment. Cell Motil Cytoskeleton 35, 121-133.
- Varma D, Monzo P, Stehman SA, Vallee RB (2008). Direct role of dynein motor in stable kinetochore-microtubule attachment, orientation, and alignment. J Cell Biol 182, 1045-1054.
- Vleugel M, Tromer E, Omerzu M, Groenewold V, Nijenhuis W, Snel B, Kops GJ (2013). Arrayed BUB recruitment modules in the kinetochore scaffold KNL1 promote accurate chromosome segregation. J Cell Biol 203, 943-955.
- Wan X, O'Quinn RP, Pierce HL, Joglekar AP, Gall WE, DeLuc JG, Carroll CW, Liu S-T, Yen TJ, McEwen BF, et al. (2009). Protein architecture of the human kinetochore microtubule attachment site. Cell 13.
- Wang Y, Jin F, Higgins R, McKnight K (2014). The current view for the silencing of the spindle assembly checkpoint. Cell Cycle 13, 1694-1701.
- Winey M, O'Toole ET (2001). The spindle cycle in budding yeast. Nat Cell Biol 3, E23-E27.
- Wynne DJ, Funabiki H (2015). Kinetochore function is controlled by a phospho-dependent coexpansion of inner and outer components. J Cell Biol 210, 899-916.
- Yamagishi Y, Yang CH, Tanno Y, Watanabe Y (2012). MPS1/Mph1 phosphorylates the kinetochore protein KNL1/Spc7 to recruit SAC components. Nat Cell Biol 14, 746-752.
- Zhang G, Kruse T, Lopez-Mendez B, Sylvestersen KB, Garvanska DH, Schopper S, Nielsen ML, Nilsson J (2017). Bub1 positions Mad1 close to KNL1 MELT repeats to promote checkpoint signalling. Nat Commun 8, 15822.